NASA/TP–2010-216168

A Deterministic Transport Code for Space Environment Electrons

John E. Nealy
Old Dominion University Research Foundation, Norfolk, Virginia

C. K. Chang
Christopher Newport University, Newport News, Virginia

Ryan B. Norman
University of Tennessee, Knoxville, Tennessee

Steve R. Blattnig
NASA Langley Research Center, Hampton, Virginia

Francis F. Badavi
Christopher Newport University, Newport News, Virginia

Anne M. Adamczyk
University of Tennessee, Knoxville, Tennessee

January 2010

NASA STI Program . . . in Profile

Since its founding, NASA has been dedicated to the advancement of aeronautics and space science. The NASA scientific and technical information (STI) program plays a key part in helping NASA maintain this important role.

The NASA STI program operates under the auspices of the Agency Chief Information Officer. It collects, organizes, provides for archiving, and disseminates NASA's STI. The NASA STI program provides access to the NASA Aeronautics and Space Database and its public interface, the NASA Technical Report Server, thus providing one of the largest collections of aeronautical and space science STI in the world. Results are published in both non-NASA channels and by NASA in the NASA STI Report Series, which includes the following report types:

- TECHNICAL PUBLICATION. Reports of completed research or a major significant phase of research that present the results of NASA programs and include extensive data or theoretical analysis. Includes compilations of significant scientific and technical data and information deemed to be of continuing reference value. NASA counterpart of peer-reviewed formal professional papers, but having less stringent limitations on manuscript length and extent of graphic presentations.

- TECHNICAL MEMORANDUM. Scientific and technical findings that are preliminary or of specialized interest, e.g., quick release reports, working papers, and bibliographies that contain minimal annotation. Does not contain extensive analysis.

- CONTRACTOR REPORT. Scientific and technical findings by NASA-sponsored contractors and grantees.

- CONFERENCE PUBLICATION. Collected papers from scientific and technical conferences, symposia, seminars, or other meetings sponsored or co-sponsored by NASA.

- SPECIAL PUBLICATION. Scientific, technical, or historical information from NASA programs, projects, and missions, often concerned with subjects having substantial public interest.

- TECHNICAL TRANSLATION. English-language translations of foreign scientific and technical material pertinent to NASA's mission.

Specialized services also include creating custom thesauri, building customized databases, and organizing and publishing research results.

For more information about the NASA STI program, see the following:

- Access the NASA STI program home page at *http://www.sti.nasa.gov*

- E-mail your question via the Internet to help@sti.nasa.gov

- Fax your question to the NASA STI Help Desk at 443-757-5803

- Phone the NASA STI Help Desk at 443-757-5802

- Write to:
  NASA STI Help Desk
  NASA Center for AeroSpace Information
  7115 Standard Drive
  Hanover, MD 21076-1320

NASA/TP–2010-216168

A Deterministic Transport Code for Space Environment Electrons

John E. Nealy
Old Dominion University Research Foundation, Norfolk, Virginia

C. K. Chang
Christopher Newport University, Newport News, Virginia

Ryan B. Norman
University of Tennessee, Knoxville, Tennessee

Steve R. Blattnig
NASA Langley Research Center, Hampton, Virginia

Francis F. Badavi
Christopher Newport University, Newport News, Virginia

Anne M. Adamczyk
University of Tennessee, Knoxville, Tennessee

National Aeronautics and
Space Administration

Langley Research Center
Hampton, Virginia 23681-2199

January 2010

Available from:

NASA Center for AeroSpace Information
7115 Standard Drive
Hanover, MD 21076-1320
443-757-5802

Nomenclature

Mathematical Constants

C_γ	$\equiv 2e^{-\gamma}$	1.122919...
e	base of natural logarithms	2.7182818...
γ	Euler's constant	0.577215665...
π	circumference/diameter ratio	3.14159265...

Physical Constants

c	speed of light in vacuum	$2.99792458 \times 10^{10}$ cm/s
e	electric charge	$1.602176487 \times 10^{-19}$ C
h	Planck constant	6.6261×10^{-27} erg s
$\hbar$	Planck constant, reduced, $\equiv h/2\pi$	1.0546×10^{-27} erg s
m_e	electron rest mass	9.1094×10^{-28} g
N_0	Avogadro's constant	6.0221×10^{23} particles/mol
r_e	classical electron radius	2.8179×10^{-13} cm
α	fine structure constant	7.2974×10^{-3}

General Variables Note: if units are not specified, then the quantity is unitless.

A	atomic mass (g/mole)
A_P	curve-fit parameter (MeV^{-p})
A_{pp}	pair production curve-fit parameter (cm^2/g)
A_S	annihilation factor in positron production term
A_T	positron annihilation loss term
A_w	curve-fit parameter used in energy straggling (MeV)
a, b	redefinition variables
a'	energy parameter
a_i	moments of scattering power for electron transport $(\text{g}/\text{cm}^2)^i$
a_H	parameter used to define the density effect correction to the Bethe-Bloch formula
C	term in modified Bethe-Bloch formula
C_E	parameter used to define applicability of density correction term to Bethe-Bloch formula
D	absorbed radiation dose (Sv)
d_i	depth in the material slab of the ith point (g/cm^2)
E	total energy (kinetic + rest mass) (MeV)
E_p	material plasma energy (MeV)
E_4	$\equiv 4$ MeV
F	cutoff dependent correction to Bethe-Bloch formula
F_c, f_c, f_{cc}	Coulomb correction terms to bremsstrahlung cross section
f	fraction of total photon attenuation for a given process
f_1, f_2, f_3	energy functions used in the definition of the cutoff correction F

G_T	ratio of energy terms in Bethe-Bloch formula
H_ν	energy function for bremsstrahlung production
h_1, h_2	energy parameters used in the annihilation cross section
I	mean atomic ionization potential (MeV)
K	integration constant
k	curve-fit parameter
L, L'	triplet term parameters defined in Table 1
m	slope parameter for photoelectric absorption coefficient
n	number density (particles/cm^3)
N	particles per unit mass (particles/g)
P_s	electron mass scattering power (cm^2/g)
p	curve-fit parameter
Q_1, Q_2	functions in pair production cross section formula (MeV^2)
q	ratio of photon energy to electron rest mass energy
R	range of electron in given material (g/cm^2)
R'	scaled energy ratio
r	electron deflection radius (g/cm^2)
S	stopping power (MeV cm^2/g)
s	curvilinear distance traversed by an electron in a material (g/cm^2)
T	particle kinetic energy (MeV)
v	particle speed (cm/s)
W	residual energy (MeV)
w	scaled thickness of a material slab (g/cm^2)
x	position or distance (g/cm^2)
y	scaled energy variable
Y	scattering function
Z	atomic number
z	axial (projected) distance traversed (g/cm^2)
β	ratio of particle speed to the speed of light in vacuum
γ	ratio of particle total energy to rest mass energy
Δ	energy parameter (MeV)
δ	density correction term in Bethe-Bloch equation
δ_s	energy function used in determining screening functions used in bremsstrahlung cross section
δ'	density correction term in pair production cross section
ϵ	screening function in Rutherford cross section
ζ	source term (particles/(MeV g))
η	transmission function
θ	scattering angle; also, polar angle in spherical coordinates
θ_r	scattering angle ratio
κ	ratio of photon energy to electron rest mass energy
λ	shell correction term in Bethe-Bloch formula
λ_{tr}	transport mean free path (g/cm^2)

μ	photon energy deposition coefficient (cm^2/g)
ξ	bremsstrahlung triplet production variable (cm^2/g)
ρ	material density (cm^{-3})
ρ'	scaled mass density (cm^6/g^2)
ρ_S	ratio of stopping powers
σ	cross section (cm^2/g)
τ	ratio of kinetic energy to rest mass energy
Φ	Klein-Nishina correction function
φ	flux (particles/(cm^2 MeV))
ϕ	spherical coordinate azimuth angle
ϕ_1, ϕ_2	screening functions
ω	electron orbital frequency (s^{-1})
$\aleph$	deviation of transport mean free path (g/cm^2)

Subscripts

ann	refers to a positron annihilation process
B	reference to Bohr stopping power formulation
CSDA	continuous slowing down approximation
col	indicates collision process
e	refers to electrons
en	refers to energy deposition in photon transport
I	reference to average ionization potential
in	refers to an incoherent scattering process
K	refers to atomic K shell
KN	refers to Klein-Nishina formula
L	refers to atomic L-shell
l	reference to lesser (or lower) value
max	maximum allowed value
min	minimum allowed value
PE	refers to photoelectric process
pp	refers to pair production process
R	refers to Rutherford formula
rad	denotes radiative (bremsstrahlung) process
Tot	indicates summation of referenced quantities
tr	reference to transport process
u	reference to higher (upper) value
ν	refers to photons
+	reference to positron

Superscripts

(s)	indicates source quantity

(t)	indicates transmitted quantity
+,-,±	reference to positron, electron, or both (respectively)
$'$,$''$	denotes dummy integration variables

Contents

List of Figures

List of Tables

Abstract

A deterministic computational procedure has been developed to describe transport of space environment electrons in various shield media. This code is an upgrade and extension of an earlier electron code. Whereas the former code was formulated on the basis of parametric functions derived from limited laboratory data, the present code utilizes well established theoretical representations to describe the relevant interactions and transport processes. The shield material specification has been made more general, as have the pertinent cross sections. A combined mean free path and average trajectory approach has been used in the transport formalism. Comparisons with Monte Carlo calculations are presented.

1 Introduction

The concept of developing a rapid analysis electron transport code at NASA Langley Research Center (LaRC) arose from a desire to have a companion code for the LaRC deterministic ion code HZETRN [1]. The initial effort resulted in a code [2] incorporating parameterizations of the effective range of electrons. These parametric functions were derived from experimental range data for electron beams incident on a variety of materials. In addition, interpolation and extrapolation methods were used in the transport computational process. Although numerous comparison calculations indicated that the code was reasonably accurate for low Earth orbit (LEO) conditions, the limit of applicability was dictated by the data range on which the code algorithms were based. Applications to gas giant planet missions with very high energy trapped electron environments required questionable extrapolation with regard to both energy and shield composition. Thus, work on a substantial upgrade began and has resulted in the new formulation described herein.

In the new code, the parametric effective range approach has been replaced in favor of a continuous slowing down approximation (CSDA) combined with an elastic multiple scattering formulation to define an electron mean free path and a transmission function at a given target location. The cross sections relevant to CSDA and multiple scattering are described in the following section. The pertinent cross sections are calculated with well established theoretical models, valid over a much greater energy range than were the expressions in the earlier code. Consequently, a calculation of positron production and annihilation has been incorporated. The cross section equations are cast in terms of specific elemental atomic species, from which cross sections applicable to any user defined molecular system are automatically constructed. Maximum accuracy would be obtained with an attachment of tabular cross section data, which are available from NIST or other sources. Databases inclusive of all elements would be inherently large and require coding to enable appropriate table look-up procedures. For the present version, the sacrifice of some precision for the sake of speed is warranted. Future versions of the code may be equipped with options to include tabular cross section data as desired by the user.

Details of the transport formulation are described in a subsequent section and are based on motion related to some initial direction (or axis of propagation). Behavior of the slowing and stopping of electrons and their associated bremsstrahlung is evaluated in terms of quantities

contained in the direction of the hemisphere centered on the initial direction. The scattering and mean free path calculations permit definition of mean trajectories, relative to the initial motion direction, so that axisymmetric spatial and energy distributions may be inferred.

Comparisons with corresponding Monte Carlo calculations are shown. The Monte Carlo cases utilized several hours of machine time, whereas the LaRC calculations were practically instantaneous. Despite some difference in final magnitudes, general functional behavior was consistent in the results, which means the use of the deterministic code in trade studies could be performed quickly and credibly. A further improvement in the present code is that the required input has been greatly simplified. The present code includes an atomic database permanent file and requires two user defined files specifying material composition along with the incident environment differential energy spectra for electrons and photons. Most results are presented for the selected materials: aluminum (Al), tantalum (Ta), and water (H_2O). This selection of target materials was chosen to provide examples of light and heavy materials in addition to elemental and compound materials. The materials were also chosen for their uses in space applications. Aluminum is a common spacecraft structural material, water closely approximates human tissue, and tantalum is used in shielding sensitive electronics from electron and photon exposure in the planetary trapped radiation belts.

2 Cross Sections

The theoretical description of the propagation of energetic electrons and photons in condensed media ordinarily requires some representation of interaction cross sections (or associated parameters) with constituent atoms of the medium. Application of the principles of quantum and semi-classical physics have gone far toward providing formulations for electron and photon interaction cross sections. Although many of these formulations are mathematically complicated, they are often amenable to approximation and parameterizations that greatly simplify their practical application. The following subsections describe the formulations used for interactions of electrons and photons.

2.1 Electrons

Free energetic electrons passing through a material are slowed and may eventually be stopped as they interact with the electric fields of nuclei and the bound electrons of the material. Interactions also result in a change of direction (scattering). In the present analysis, the electron deceleration process is expressed in terms of energy loss by collisions and accompanying photon production (bremsstrahlung). The dominant scattering process is assumed to be that of small angle elastic (Rutherford) scattering. It is the only scattering process taken into account in the present formulation.

2.1.1 Collisional Slowing and Stopping

Electron deceleration by collision processes, in which energy from the projectile electron is imparted to the electrons of the medium, is usually cast in terms of the stopping power, S, which is the energy loss per unit scaled distance, $-dE/dx$. Note that the distance x is measured

in units of g/cm^2. The resultant expression has been often referred to as the modified Bethe-Bloch formula and is given here in the notation of Ref. [3],

$$S_{\rm col} \equiv \frac{dE}{dx} = 2\pi r_e^2 m_e c^2 \rho' (N_0 Z/A) G_T C^{\pm}, \tag{1}$$

where

$$G_T = \frac{(T + m_e c^2)^2}{T(T + 2m_e c^2)}$$

and

$$C^{\pm} = \left\{ \ln \left[\frac{2(T + 2m_e c^2)}{m_e c^2 (I/m_e c^2)^2} \right] + F^{\pm} - \delta - \lambda \right\}. \tag{2}$$

The superscript ($\pm$) indicates applicability to both electrons (-) and positrons (+). Here, I is the mean atomic ionization potential, m_e is the rest mass of the electron, c is the speed of light in vacuum, ρ' is the scaled mass density with distance measured in g/cm^2, N_0 is Avogadro's constant, Z is the atomic number of the material, A is the atomic mass of the material, r_e is the classical electron radius, T is the kinetic energy of the electron or positron, δ is the density correction term, and λ is the shell correction term. The $F^{\pm}$ quantity in Eq. (2) is a function only of projectile energy and is slightly different (a few percent) for electrons and positrons. The present formulation implements only the $F^{\pm}$ function that applies to electrons. It may be written as the sum of three terms,

$$F^{\pm} \approx F^{-} = f_1 + f_2 - f_3, \tag{3}$$

where

$$f_1 = \frac{T}{T - \Delta} + \ln \left[\frac{\Delta(T - \Delta)}{(m_e c^2)^2} \right],$$
$$f_2 = \frac{\Delta^2/2 + m_e c^2 (2T + m_e c^2) \ln(1 - \Delta/T)}{(T + m_e c^2)^2},$$
$$f_3 = 1 + \frac{T(T + 2m_e c^2)}{(T + m_e c^2)^2},$$

and

$$\Delta = T/2.$$

The quantity δ in Eq. (2) represents a modification to the Bethe-Bloch stopping power usually referred to as the "density correction" and is presented in detail in Ref. [4]. The formulation of

this correction term is based on extensive experimental data and is highly parameterized. The energy conditional relationships are cast in terms of an energy variable,

$$y \equiv \log_{10}(\gamma\beta) = \frac{\ln(\gamma^2\beta^2)}{2\ln(10)} = \frac{\ln\left[(T^2 + 2Tm_ec^2)/(m_ec^2)^2\right]}{2\ln(10)}, \tag{4}$$

where β is the ratio of the electron speed to the speed of light and $\gamma \equiv 1 + T/m_ec^2$. The elemental "plasma energy," E_p, also enters into the formulation. Its value is given by

$$E_p = \hbar c\sqrt{4\pi r_e \rho(N_0 Z/A)} \tag{5}$$

and appears in the parameter C_E. Here, $\hbar$ is the reduced Planck constant and ρ is the material density. The parameter C_E is given as

$$C_E = 1 + 2\ln(I/E_p), \tag{6}$$

where I is the mean atomic ionization potential. The C_E parameter is used in conjunction with other parameters to define limits of application to the δ correction term. The value of δ is defined by

$$\delta \equiv \begin{cases} 0 & y < y_0 \\ 4.60517y - C_E + a_H(y_1 - y)^3 & y_0 \le y \le y_1 \\ 4.60517y - C_E & y_1 < y \end{cases} \tag{7}$$

and applies for electron energies ≥ 0.0001 MeV (or 100 eV). The parameters y_0, y_1, and a_H are defined as

$$\begin{aligned} y_0 &\equiv \begin{cases} 0.2 & C_E \le 5.215 \\ 0.326C_E - 1.5 & C_E > 5.215 \end{cases}, \\ y_1 &\equiv 3.0, \\ a_H &\equiv 4.60517(y_a - y_0)/(y_1 - y_0)^3, \\ y_a &\equiv C_E/2\ln(10) = C_E/4.60517. \end{aligned}$$

The remaining correction term, λ, in Eq. (2), is called the "shell correction" and is only important at low energies when the projectile electron speed, v, approaches the speed of a bound electron, v_I. Its value, as used in the present calculations, is given by [5]

$$\lambda \approx \left(\frac{v_I}{v}\right)^2 \approx \frac{I(I + 2m_ec^2)(T + m_ec^2)^2}{T(T + 2m_ec^2)(I + m_ec^2)^2}. \tag{8}$$

It is seen in Eq. (1) that S_{col} is unbounded as $T \to 0$ due to the G_T factor. An early non-relativistic stopping power derivation was provided by Bohr [5], which approached zero

at very low energies and exhibited a maximum. The Bohr formula may be written in CGS (centimeters-grams-seconds) units as

$$S_{\rm Bohr} = \frac{4\pi n e^4}{m_e v^2} \ln\left(\frac{C_\gamma m_e v^3}{e^2 \omega_I}\right) \equiv \frac{a}{T} \ln\left(bT^{3/2}\right), \tag{9}$$

with $C_\gamma = 2{\rm e}^{-\gamma}$ and $\omega_I = I/\hbar$. From $\frac{dS_{\rm Bohr}}{dT} = 0$,

$$\ln\left(bT_B^{3/2}\right) = \frac{3}{2}.$$

From Eq. (9),

$$b = 2^{3/2} C_\gamma / (e^2 \omega_I \sqrt{m_e})$$

and

$$T_B = \left(\frac{{\rm e}^{3/2} e^2 \sqrt{m_e} I}{2^{3/2} C_\gamma \hbar}\right)^{2/3},$$

where T_B is the projectile kinetic energy at peak stopping power. If Eq. (1) is compared with Eq. (9), the natural logarithm term in Eq. (9) can be identified with the $C^\pm$ in Eq. (1). This gives

$$C^\pm_{\rm max} = \ln\left(bT_B^{3/2}\right),$$
$$S_{\rm max} \equiv 2\pi r_e^2 m_e c^2 N_0 G_T (Z/A) C^\pm_{\rm max}.$$

For $T < T_B$, an extension to low energies is provided by Sigmund [5]. A simple functional fit has been derived for the present work,

$$S_{\rm col} = S_{\rm max} \ \exp\left\{-0.179 \left[\ln\left(T_B/T\right)\right]^{2.05}\right\} \quad \text{for } T < T_B \tag{10}$$

and Eq. (1) is applied for $T \geq T_B$.

Three simple materials important to space exploration applications have been selected to demonstrate results of the present model calculations: water, aluminum, and tantalum. They were chosen to represent a broad range of atomic properties and material densities. Fig. 1 depicts the collision stopping powers as calculated for these substances over the energy range of the code formulation. The most notable features are the generally higher stopping powers for lighter materials and the shift of peak stopping power to higher energy for the higher atomic number materials. For comparison, the stopping powers obtained from the database tabulations of the National Institute of Standards and Technology (NIST) [6] are also shown. The comparisons indicate that the present formulation is quite acceptable over the energy range of interest for space applications (0.001 - 1000 MeV), with the greatest discrepancies occurring at the lowest energies for heavier elements.

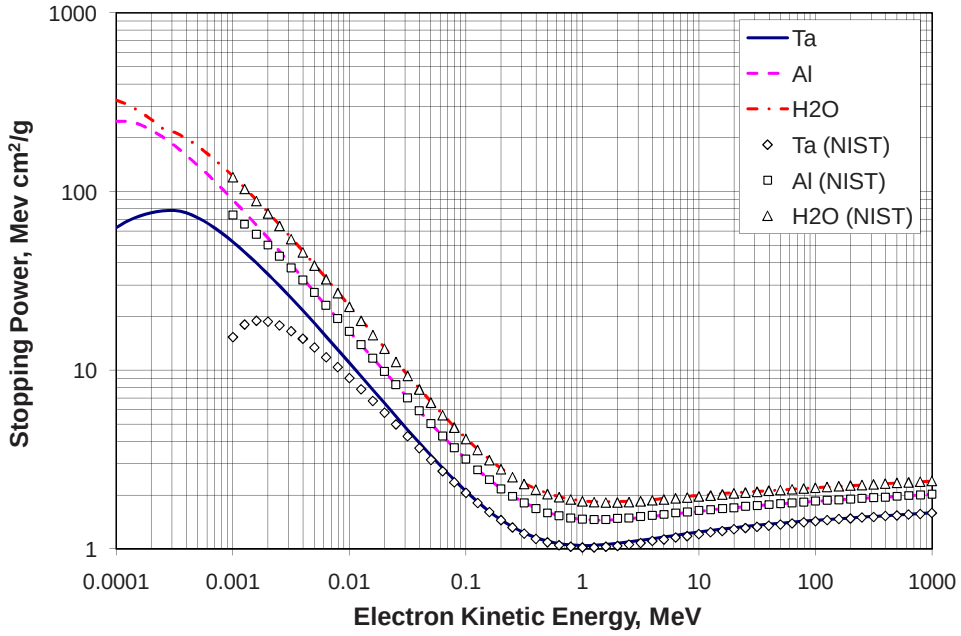

Figure 1: Collisional stopping power from current model and NIST calculations [6].

2.1.2 Radiative Energy Loss (Bremsstrahlung)

Accelerating (and decelerating) charged particles lose energy by photon emission. Elaborate quantum mechanical calculations have gone far toward quantifying bremsstrahlung cross sections. A detailed description of the theoretical results is given in Ref. [7]. The formulation may be greatly simplified by using several parameterizations; the implementation for this work is essentially the same as that for the default cross sections of the EGSnrc Monte Carlo code [8]. Several pertinent parameters that lead to the ultimate cross section formula may be defined as

$$F_c \equiv 4\left[\frac{1}{3}\ln(Z) + f_c\right], \tag{11}$$

where

$$f_c \equiv \begin{cases} 0.0 & E_\nu < 50 \text{ MeV} \\ f_{cc} & E_\nu \geq 50 \text{ MeV} \end{cases},$$

with

$$f_{cc} \equiv (\alpha Z)^2 \sum_{n=1}^{\infty} \frac{1}{n(n^2+\alpha^2 Z^2)} \cong 7.4564 \times 10^{-5} Z^{1.9137}.$$

Here, α is the fine structure constant. The term F_c serves to provide a high energy Coulomb correction. Another parameter defines the effects of screening in terms of an energy variable,

$$\delta_s = \left(\frac{136}{Z^{1/3}}\right)\left[\frac{E_\nu m_e c^2}{E_e(E_e - E_\nu)}\right],$$

which involves the electron total energy, $E_e = T + m_e c^2$, and the emitted photon energy, E_ν. The screening functions have been specified as [8]

$$\phi_1(\delta_s) = \begin{cases} 20.867 - 3.242\delta_s + 0.625\delta_s^2 & \delta_s \leq 1 \\ 21.12 - 4.184\ln(\delta_s + 0.952) & \delta_s > 1 \end{cases}, \tag{12}$$

$$\phi_2(\delta_s) = \begin{cases} 20.209 - 1.935\delta_s + 0.086\delta_s^2 & \delta_s \leq 1 \\ \phi_1(\delta_s) & \delta_s > 1 \end{cases}.$$

A final parameter, ξ, which accounts for the triplet production process, depends upon atomic charge and involves the Coulomb correction above, along with the quantities L and L' that have been tabulated in Ref. [8] and are given in Table 1. A parameterized fit for ξ has been developed for this work,

$$\xi = L'/(L - f_c) \approx 1.147\sin(0.42\ln\ Z) + 0.12\left\{[\sin(0.76\ln\ Z)]^2\right\}^{3/4}. \tag{13}$$

The final expression for the cross section for production of a photon of energy E_ν by interaction of an electron of total energy E_e on an atom of charge Z may be written as

$$\frac{d\sigma_{\nu,e}}{dE_\nu} = \frac{\alpha r_e^2}{E_\nu}\frac{N_0 Z(Z+\xi)}{A}H_\nu, \tag{14}$$

where

$$H_\nu = \left\{\left[1 + \left(\frac{E_e - E_\nu}{E_e}\right)^2\right](\phi_1 - F_c) - \frac{2}{3}\left(\frac{E_e - E_\nu}{E_e}\right)(\phi_2 - F_c)\right\}.$$

An obvious energy constraint is that only photons can be produced that have energy less than the initial electron kinetic energy. Consequently, $d\sigma_{\nu,e}/dE_\nu$ is calculated at each electron energy T, for selected values of E_ν/T: [0.001, 0.05, 0.1, 0.2, 0.3, 0.4, 0.6, 0.8, 0.9, 0.95, 0.98, 0.99, 1.0]. This array has been chosen because the cross section variations are greater at either end of the energy range. A source term ζ, for production of photons by an electron flux φ_e, may be written in terms of the bremsstrahlung cross section as

$$\zeta(E_\nu, T) = \int_{E_\nu}^{T} \varphi_e(T')\frac{d\sigma_{\nu,e}}{dE_\nu}dT' \text{ for } E_\nu \leq T. \tag{15}$$

Table 1: Parameter values used in Eq. (13) from Ref. [8].

Z	L	L'
1	5.31	6.144
2	4.79	5.621
3	4.74	5.805
4	4.71	5.924
> 4	$\ln(184.15Z^{-1/3})$	$\ln(1194Z^{-2/3})$

The corresponding energy loss term due to radiative processes may be evaluated as

$$S_{\rm rad} = \int_0^{E_\nu} E'_\nu \frac{d\sigma_{\nu,e}}{dE'_\nu} dE'_\nu. \tag{16}$$

Radiative loss stopping powers for the three materials selected for illustration are shown in Fig. 2. In contrast to the collision stopping powers, bremsstrahlung stopping power is greater for higher charge elements and increases monotonically with energy. The logarithmic stopping power for the present approximate formulation is very nearly linear with the logarithm of the energy and begins to have substantial effects only for kinetic energies greater than a few MeV. Comparison with NIST data reveals substantial disparities at low kinetic energies, but, as will be shown subsequently, bremsstrahlung effects on the general transport process have a significant impact only for kinetic energies greater than several MeV.

2.1.3 Multiple elastic scattering

Strict conservation principles require that electron-atom interactions generally result in energy exchange accompanied by re-direction with respect to spatial variables. Approximations that tend to decouple energy loss processes and directional changes greatly simplify electron transport analysis. In the present work, these processes are made practically independent. Energy loss is specified by collision and radiative losses without regard for directional change, while projectile trajectories are described by elastic scattering interactions. Such drastic assumptions call for careful scrutiny with regard to both broad energy spectra and the wide variety of material types. Some precedents have been set in earlier works [9, 10] in which such approaches have been used. In the present formulation, the elastic (Rutherford) scattering cross sections, $\sigma_{\rm R}$, are implemented as a basis for calculating an electron transport mean free path,

$$\lambda_{\rm tr} \equiv \frac{\rho}{n\sigma_{\rm R}}, \tag{17}$$

where $n = \rho N_0/A$ is the number of scattering centers per unit volume in the medium. See Section 3.1 and Ref. [10] for further discussion on transport mean free path. Notice that $\lambda_{\rm tr}$ is defined to have units of g/cm^2. The present development closely follows that of Ref. [8]. The screened Rutherford cross section is given as

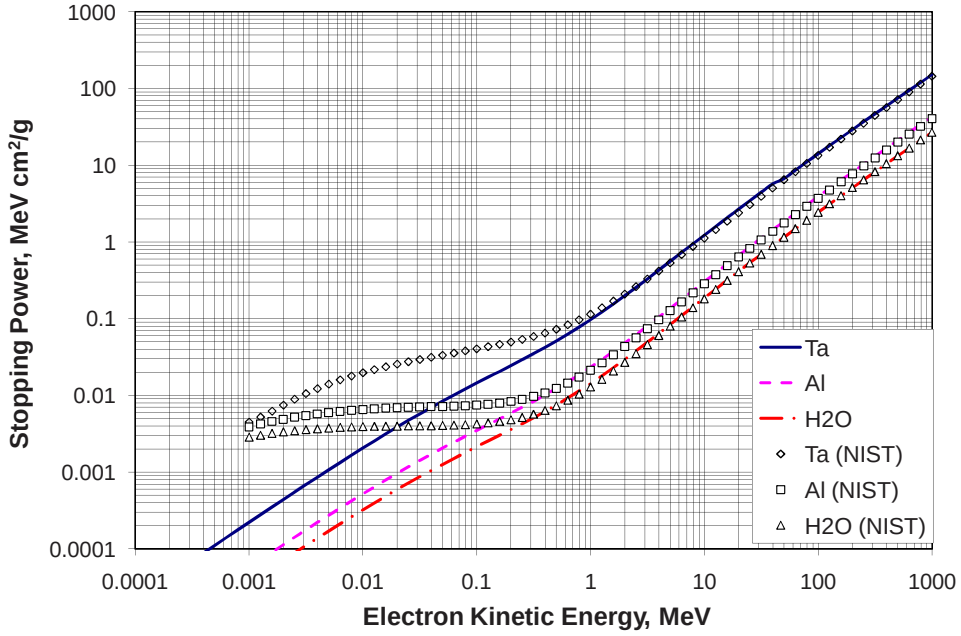

Figure 2: Radiative stopping power from current model and NIST calculations [6].

$$\frac{d\sigma_{\rm R}}{d\theta} \equiv 2\pi \left[\frac{Ze^2}{(T+m_ec^2)\beta^2(1-\cos\theta+1/\epsilon)}\right]^2, \tag{18}$$

where θ is the scattering angle and ϵ is a parameterized screening function,

$$\epsilon \approx 1413[(1+T/m_ec^2)^2-1](Z\alpha)^{-2/3}.$$

The total cross section is found by integration over all scattering angles.

$$\sigma_{\rm R} = \int_{-1}^{1} \frac{d\sigma_{\rm R}}{d\theta}(1-\cos\theta)d\cos\theta. \tag{19}$$

The integral may be readily evaluated with the substitutions $x \equiv \cos\theta$ and $K \equiv 1+1/\epsilon$, to give

$$\begin{aligned}\int_{-1}^{1} \frac{1-x}{(K-x)^2}dx &= \ln\left(\frac{K+1}{K-1}\right) - \left[1+\frac{K-1}{K+1}\right] \\ &= \ln(2\epsilon+1) - \frac{2(\epsilon+1)}{2\epsilon+1} \\ &\approx \ln(2\epsilon) - 1 \text{ for } \epsilon \gg 1.\end{aligned}$$

The reciprocal of the transport mean free path, $n\sigma_{\mathrm{R}}/\rho$, may be expressed in terms of kinetic energy as

$$\frac{n\sigma_{\mathrm{R}}}{\rho} = \frac{N_0}{A}\sigma_{\mathrm{R}} = \frac{N_0}{A}\frac{2\pi Z^2 e^4}{(T + m_e c^2)^2 \beta^4}\left[\ln(2\epsilon) - 1\right]. \tag{20}$$

Using expressions from special relativity, terms in the denominator of Eq. (20) may be cast in terms of electron kinetic energy.

$$\begin{aligned}
\tau &\equiv T/m_e c^2, \\
\beta^2 &\equiv \frac{\tau^2 + 2\tau}{(\tau+1)^2}, \\
(T + m_e c^2)^2 \beta^4 &= (m_e c^2)^2 \left[\frac{(\tau+1)^4 - 2(\tau+1)^2 + 1}{(\tau+1)^2}\right] \\
&= T^2 + 2T m_e c^2 - (m_e c^2)^2 + \frac{(m_e c^2)^4}{(T + m_e c^2)^2}.
\end{aligned}$$

Now, the electron transport mean free path becomes

$$\lambda_{\mathrm{tr}} \equiv \rho/n\sigma_R = \frac{A}{2\pi N_0 e^4 Z^2}\left[\frac{T^2 + 2T m_e c^2 - (m_e c^2)^2 + (m_e c^2)^4/(T + m_e c^2)^2}{\ln(2\epsilon) - 1}\right]. \tag{21}$$

Note that the behavior of the transport mean free path increases monotonically with kinetic energy, is nearly logarithmically linear with the log of the kinetic energy, and has generally higher values for lower atomic weight elements.

Another parameter related to elastic multiple scattering is the mass scattering power [11]. This quantity is analogous to stopping power, but refers to solid angle scattering rather than energy loss. The mass scattering power is defined in Ref. [11] as

$$P_s \equiv \pi\left[\frac{2r_e Z}{\beta^2(\tau+1)}\right]^2 \frac{N_0}{Z} Y(\theta_r), \tag{22}$$

where

$$\theta_r = \frac{\sqrt{\tau^2 + 2\tau}}{\alpha Z^{1/3}}$$

with

$$Y(\theta_r) \equiv \ln(1 + \theta_r^2) - 1 + \frac{1}{1 + \theta_r^2}.$$

The mass scattering power is used in the transport algorithm to relate electron traversal on a specific trajectory to the axial penetration distance. The above formulation predicts a nearly linear monotonically decreasing variation of the logarithm of scattering power with the logarithm of energy.

2.2 Photons

Bremsstrahlung photons produced by electron-atom interactions are attenuated and absorbed in the transport medium. In the present work, only the three most important processes involved in photon energy degradation and absorption are considered: (1) photoelectric absorption, (2) incoherent scattering, and (3) positron-electron pair production. These processes are dominant for different energy ranges, but when taken collectively they closely approximate the total attenuation for the energy range considered here (0.001 - 1000 MeV). The contribution due to coherent (or Rayleigh) scattering has not been included in this analysis since it does not significantly add to the total cross section over the energy range of interest (0.001 - 1000 MeV).

2.2.1 Photoelectric Absorption

Photoelectric absorption involves interactions of a photon with a bound electron in which the photon energy is absorbed with a corresponding kinetic energy increase for the electron. The detailed evaluation of the photoelectric cross sections requires the use of complicated atomic models in sophisticated solutions of the Schrödinger equation for all energies and elements under consideration. For the present formulation, liberal use is made of parametric fitting formulas devised from the extensive calculations and tabulations provided by NIST [6]. First, the photon energy values for the absorption discontinuities of the K and L shells have been approximated as

$$\begin{aligned} E_K &\approx 5.435 \times 10^{-3} Z^{2.2038} \quad \text{keV} \qquad (1 \leq Z \leq 92), \\ E_L &\approx 1.5754 \times 10^{-4} Z^{2.5984} \quad \text{keV} \qquad (30 \leq Z \leq 92). \end{aligned} \tag{23}$$

Note that energies in this section are in keV and L-edge energies are only considered for $Z \geq 30$. In addition, only the discontinuities due to the K and L shells have been considered. The discontinuities (or edges) due to the electronic shells occur at values of the photon energy corresponding to the binding energies of electrons involved in the interaction. When the incoming photon has an energy greater than the binding energy of a given atomic shell or subshell, a discontinuity may occur.

At the edge discontinuities, the NIST data has also been used to develop formulas for the upper (u) and lower (l) values of the photoelectric cross section:

$$\begin{aligned} \sigma_{Ku} &= 7165.5 E_K^{-1.5474} \qquad \text{cm}^2/\text{g}, \\ \sigma_{Kl} &= 593.59 E_K^{-1.327} \qquad \text{cm}^2/\text{g}, \\ \sigma_{Lu} &= 9620.6 E_L^{-1.5113} \qquad \text{cm}^2/\text{g}, \\ \sigma_{Ll} &= 1633.5 E_L^{-1.2124} \qquad \text{cm}^2/\text{g}. \end{aligned} \tag{24}$$

Examination of typical photoelectric cross sections reveals that the logarithmic slope,

$$m \equiv \frac{d(\ln\ \sigma_{\text{PE}})}{d(\ln\ E_\nu)},$$

is very nearly constant for a given atomic system between absorption edges. Again, using NIST cross section data, parametric fits have been used to approximate the logarithmic slopes.

For $E_\nu > E_K$:

$$m_K = \begin{cases} 6.9068 \times 10^{-3} Z - 3.014 & Z \leq 10 \\ -3.3147 Z^{-0.08156} & Z \geq 11 \end{cases} . \tag{25}$$

For .1 keV $\leq E_\nu \leq E_K$:

$$m_L = \frac{\ln\left(\frac{\sigma_{Kl}}{\sigma_{Lu}}\right)}{\ln\left(\frac{E_K}{E_L}\right)}.$$

For all Z and $E_K < E_\nu < 10000$ keV:

$$\sigma_{\mathrm{PE}} = \sigma_{Ku} \left(\frac{E_\nu}{E_K}\right)^{m_K} . \tag{26}$$

For $Z \geq 29$ and $E_L < E_\nu < E_K$:

$$\sigma_{\mathrm{PE}} = \sigma_{Lu} \left(\frac{E_\nu}{E_L}\right)^{m_L} .$$

An extension to energies less than the lowest edge energy considered is extrapolated with a power law function approaching an asymptote based on an extrapolated maximum absorption cross section. For $Z \leq 29$ and for energies below the K-edge, an asymptotic cross section is calculated using the average ionization potential,

$$\sigma_I = \sigma_{Kl} \left(\frac{I}{E_K}\right)^{m_K} . \tag{27}$$

The extrapolation formula is then

$$\sigma_{\mathrm{PE}} = \frac{\sigma_I}{1 + A_P E_\nu^p}, \tag{28}$$

where the constants are given by

$$p = \frac{m_K}{(\sigma_{Kl}/\sigma_I) - 1}; \quad A_P = \frac{(\sigma_I/\sigma_{Kl}) - 1}{E_K^p}. \tag{29}$$

These constants are found by matching the cross section and the slope at the K-edge. For $Z \geq 29$, the low energy extrapolation below the L-edge is found by using a L subscript instead of K in Eqs. (26)-(29).

The photoelectric cross sections, as calculated with the present highly parametric formulation, are shown in Fig. 3 for the three selected materials along with their NIST counterparts. Agreement is considered to be fair to good. In circumstances for which low energy photon extinction is deemed important, it would probably be best to introduce a tabular database for interpolation.

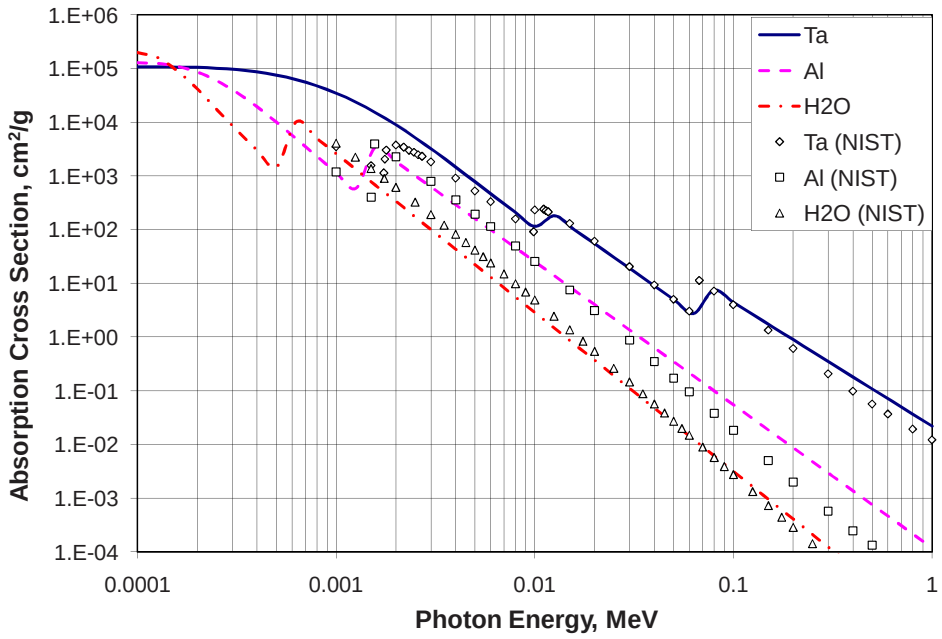

Figure 3: Photoelectric absorption cross sections from the current model and NIST calculations [6].

2.2.2 Inelastic Photon Interactions

As the photoelectric absorption coefficient decreases rapidly with increasing energy, the next process to dominate is when the photon imparts a part of its energy to an electron resulting in scattering of a lower energy photon. The process is referred to as inelastic (or incoherent) scattering. The cross section formula for release of an electron of kinetic energy T_e by a photon of initial energy E_ν has been taken from Ref. [3] as the free electron Klein-Nishina process. The energy constraints are

$$
\begin{aligned}
&0 \leq T_e \leq T_{\max};\\
&T_{\max} = \frac{2qE_\nu}{1+2q},\\
&q \equiv \frac{E_\nu}{m_e c^2},
\end{aligned}
$$

where T_e is the kinetic energy of the emitted electron and E_ν is the incident photon energy. The cross section formulation is

$$\begin{aligned}
\frac{d\sigma_{\mathrm{KN}}}{dT_e} &= \frac{N_0 Z}{A}\frac{\pi r_e^2}{qE_\nu}\left\{2+\frac{T_e^2}{(E_\nu-T_e)^2}\left[\frac{1}{q^2}+\frac{E_\nu-T_e}{E_\nu}-\frac{2(E_\nu-T_e)}{qT_e}\right]\right\} \\
&= \frac{N_0 Z}{A}\frac{\pi r_e^2}{qE_\nu}\left[2+\left(\frac{R'}{q}\right)^2+\frac{R'T_e}{E_\nu}-\frac{2}{qR'}\right]; \\
R' &\equiv \frac{T_e}{E_\nu-T_e}.
\end{aligned} \tag{30}$$

In order to render the cross section applicable to bound atomic electrons, elaborate quantum theory calculations are required. Such considerations are only appreciable at lower photon energies. For this work, a parametric multiplying function has been developed to approximate this effect.

$$\ln\ \Phi(Z,E_\nu) = -\left[\frac{0.471\ \ln(Z)+1.5184}{E_\nu}\right]^{[1.003-0.13317\ln(Z)]}. \tag{31}$$

The final inelastic scattering cross section then becomes

$$\frac{d\sigma_{\mathrm{in}}}{dT_e} = \Phi(Z,E_\nu)\frac{d\sigma_{\mathrm{KN}}}{dT_e}. \tag{32}$$

For each E_ν, the total inelastic cross section is found by integration over the appropriate emitted electron energy.

$$\sigma_{\mathrm{in}} = \int_0^{T_{\max}} \frac{d\sigma_{\mathrm{in}}}{dT'}dT'. \tag{33}$$

The total inelastic cross sections calculated with the present model are plotted as a function of incident photon energy in Fig. 4 along with the corresponding NIST values. The model works better for light materials compared to heavy materials and begins to fail at high energies for all materials. In this energy range, the inelastic cross section does not contribute appreciably to the total photon attenuation, as will be subsequently shown.

2.2.3 Pair Production

Electron-positron pair production may occur when a photon of sufficient energy interacts with a strong localized Coulomb field. The photon initial energy is transformed into the combined rest mass ($2m_ec^2$) of the newly created particles. Any remaining energy appears as kinetic energy of the new particles. A comprehensive description of the process may be found in Ref. [12], where a variety of cross section quantities are derived for several aspects of the phenomenon. The formulation from Ref. [11], chosen for use in the present work, applies to the cross section

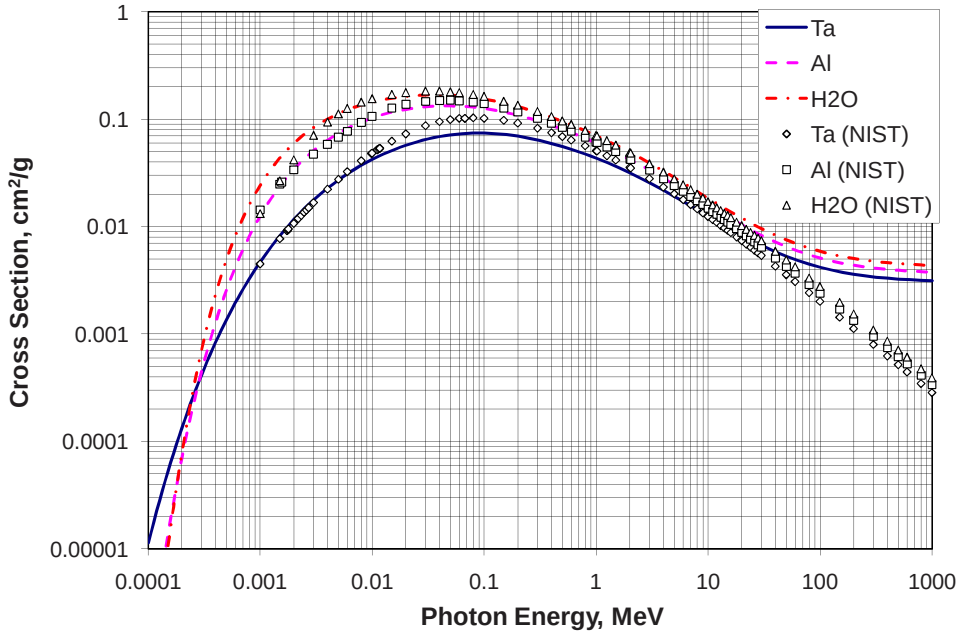

Figure 4: Inelastic photon cross sections from the current model and NIST calculations [6].

for production of a positron of total energy E_+ by a photon of initial energy E_ν. Only positron production associated with pair production is considered in this work. The pair production differential cross section may be written in simple terms as

$$\frac{d\sigma_{\rm pp}}{dE_+} = \frac{N_0}{A}\frac{\alpha r_e^2 Z(Z+\xi)}{E_\nu^3}(Q_1+Q_2), \tag{34}$$

where

$$Q_1 = [E_+^2 + (E_\nu - E_+)^2][\phi_1 - F_c],$$
$$Q_2 = \frac{2}{3}E_+(E_\nu - E_+)[\phi_2 - F_c].$$

The terms ξ, $\phi_1(\delta')$, $\phi_2(\delta')$ and F_c are the same as for the bremsstrahlung cross section, Eqs. (11)-(13), with the exception that the value of δ' is determined as

$$\delta' = \frac{136 m_e c^2 E_\nu}{Z^{1/3}E_+(E_\nu - E_+)}. \tag{35}$$

Energy conservation constrains the positron energy as

$$m_e c^2 \le E_+ \le T_{\rm max} + m_e c^2,$$
$$T_{\rm max} = E_\nu - 2m_e c^2.$$

The above formulas for pair production become inaccurate as the pair production threshold is approached. Consequently, a power law function is fit at the first energy grid value greater than 4 MeV ($\equiv E_4$). Now, the low energy pair production cross section is given as

$$\sigma_{\rm pp} = A_{\rm pp}(E_\nu - 1.03)^b \quad \text{for } 1.03 < E_\nu < E_4, \tag{36}$$

with

$$b = \left.\frac{d\sigma_{\rm pp}}{dE_+}\right|_{E_+=E_4} \frac{E_4 - 1.03}{\sigma_{\rm pp}(E_4)},$$
$$A_{\rm pp} = \frac{\sigma_{\rm pp}(E_4)}{(E_4 - 1.03)^b}.$$

A source term for positron production may be derived in a manner similar to that described previously for production of bremsstrahlung photons. See Eq. (15). For a photon differential flux spectrum $\varphi_\nu(E_\nu, x)$, positron production may occur between energies $E_{\rm pp,min} = 2m_e c^2$ and $E_{\rm pp,max} = E_{\nu,\rm max} - 2m_e c^2$, where $E_{\nu,\rm max}$ is the highest photon energy value considered. The expression for the source term becomes

$$\zeta(E_+, x) = \int_{E_{\rm pp,min}}^{E_{\rm pp,max}} \varphi_\nu(E_\nu^{'}, x) \frac{d\sigma_{\rm pp}}{dE_+} dE_\nu^{'}. \tag{37}$$

It should be noted that in parallel with the positron production process, a similar cross section expression applies to the creation of the partner electron, along with the corresponding source term for secondary electrons. Just as for the inelastic process, the pair production cross section may be found by integration over the allowed positron energy ranges

$$\sigma_{\rm pp} = \int_{m_e c^2}^{E_{+,\rm max}} \frac{d\sigma_{\rm pp}}{dE_+^{'}} dE_+^{'}, \tag{38}$$

where $E_{+,\rm max} = E_\nu - m_e c^2$.

Results of pair production cross sections, as calculated from the present model, are shown in Fig. 5 along with the appropriate NIST comparison values. Agreement is very good except for energies near the threshold region where the power law extrapolation formula has been invoked.

2.3 Cross Section Implementation

The individual cross sections described previously are used in combination to provide three critical parameters essential for description of the electron-photon transport process. The ultimate slowing and stopping of electrons is governed by the total stopping power obtained from the sum of the collision and radiative stopping powers. The collision process dominates at low energies (less than approximately 1 MeV), while the radiative process assumes the dominant role

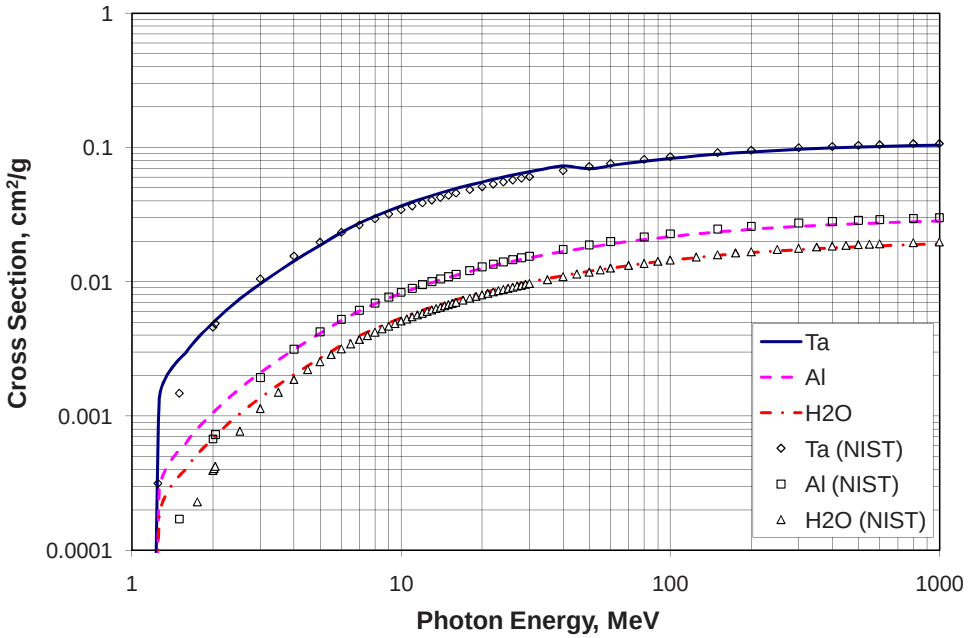

Figure 5: Pair production cross sections from current model and NIST calculations [6].

at high energies (greater than approximately 1 MeV). A transitional minimum occurs in the neighborhood of 1 MeV as is shown in Fig. 6, where the total stopping power is plotted along with the comparison values taken from Ref. [6]. Note that the lower energy inaccuracies of the model radiative stopping power have insignificant impact on the total stopping power.

The general attenuation and extinction of photons in a medium is found to be closely related to the sum of the photoelectric, inelastic, and pair production cross sections. Coherent scattering processes have not been considered because of their relative unimportance in space radiation effects. Fig. 7 shows the model total attenuation coefficient (taken to be the sum of the photoelectric, inelastic and pair production cross sections) and the selected comparison data, where the model results are again deemed satisfactory for an adequate description of the photon transport.

The final parameter of importance to the electron-photon transport process is that of the photon energy deposition coefficient which is used to calculate effective photon dose in Eq. (64). This relates to those fractions of the photon attenuation processes ($f_{\rm PE}$, $f_{\rm in}$, $f_{\rm pp}$) that produce secondary electrons. For photoelectric absorption, it is assumed that the secondary electron is emitted with the same energy as the incident photon (i.e. the binding energy of the released electron is neglected) and the value of $f_{\rm PE}$ is unity. In the case of inelastic scattering [13],

$$f_{\rm in} = 1 - \frac{E_{\nu,{\rm in}}}{E_\nu},$$

where $E_{\nu,{\rm in}}$ is the energy of the photon produced in the inelastic process initiated by a photon

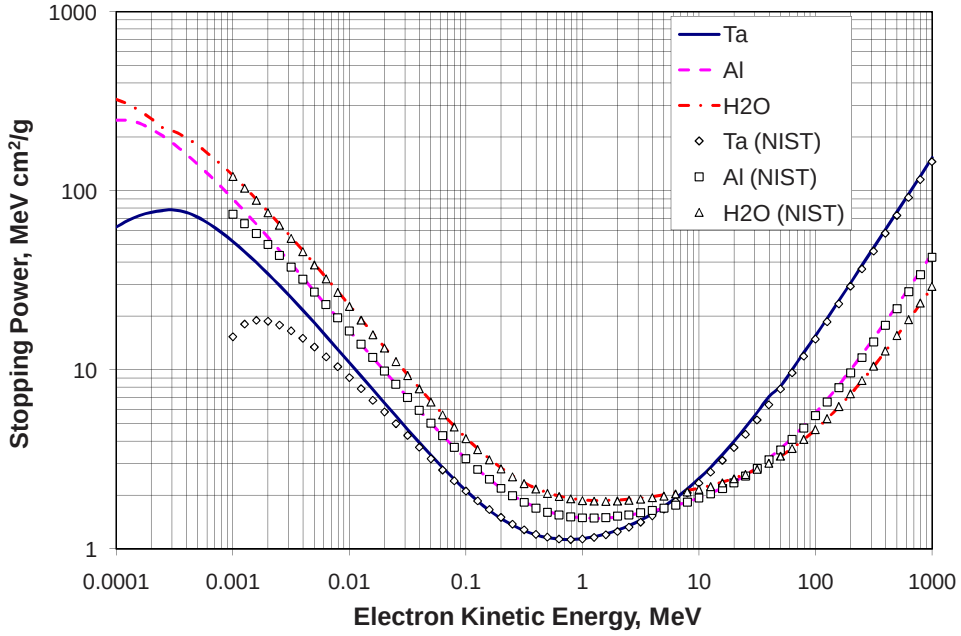

Figure 6: Model total stopping powers compared with NIST calculations [6].

of energy E_ν. For the pair production process, $f_{\rm pp} = 1 - 2m_e c^2/E_\nu$.

An additional reduction in the photon energy deposition coefficient is required to discount those secondary electrons that go on to produce additional bremsstrahlung. In the present model, this factor is represented by $(1 - S_{\rm rad}/S_{\rm Tot})$, where $S_{\rm Tot} \equiv S_{\rm rad} + S_{\rm col}$. This factor is only applied to the inelastic and pair production processes, so that the model expression for the total photon energy deposition coefficient becomes [13]

$$\mu_{\rm en} = \sigma_{\rm PE} + \int_0^{T_{\rm max,in}} (1 - \frac{S_{\rm rad}}{S_{\rm Tot}}) f_{\rm in} \frac{d\sigma_{\rm in}}{dT'} dT' + \int_0^{T_{\rm max,pp}} (1 - \frac{S_{\rm rad}}{S_{\rm Tot}}) f_{\rm pp} \frac{d\sigma_{\rm pp}}{dT'} dT', \tag{39}$$

where the upper limits on the integrations apply to the maximum allowed emitted electron energies for the respective processes. The energy deposition coefficient is described in detail in the X-Ray Data section of the NIST website [6]. A comparison of model results with the more elaborate NIST calculations is shown in Fig. 8.

3 Transport Formulation

In the present work, the general transport process is focused principally on description of penetration of a primary electron field along with secondary bremsstrahlung photons generated by electron-atom interactions. For electrons, an essentially one-dimensional formulation is developed with some reference given to the effects of radially symmetric scattering. While the electron

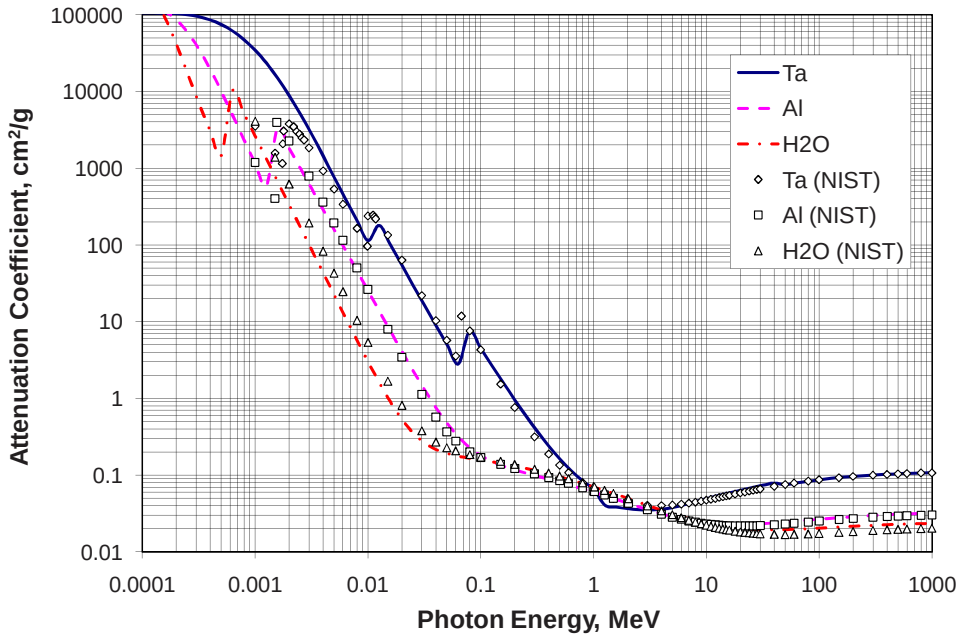

Figure 7: Model photon total attenuation coefficient compared with NIST values [6].

propagation is determined by the stopping powers, the photons are assumed to be transported along the direction of travel of the electrons. Photon intensity is governed by the radiative transfer equation [14], which utilizes the calculated attenuation coefficients.

3.1 Electrons

A quantity of fundamental importance in describing transport of electrons in matter is that of the maximum distance of travel as determined from the energy loss stopping powers calculated from the modified Bethe-Bloch and bremsstrahlung formulas in Eqs. (1) and (16). This quantity is referred to as the Continuous Slowing Down Approximation (CSDA) range $R(E)$. For a given energy, E, the CSDA range is determined from [2]

$$R(E) \equiv \int_0^E \frac{dE'}{S_{\text{Tot}}} = \int_0^E \frac{dE'}{S_{\text{col}} + S_{\text{rad}}}. \tag{40}$$

The inverse of the $R(E)$ function, $R^{-1}(E) \equiv E(R)$, may be used to construct the variation of dE/dx as a function of distance traveled by an electron of initial energy E_0. Such a function, $S(E_0, x)$, is analogous to the usual Bragg curve, but neglects straggling and measures energy loss as a function of distance traveled along the particle's path rather than perpendicular depth in a material. Straggling is accounted for after the incorporation of the statistics associated with

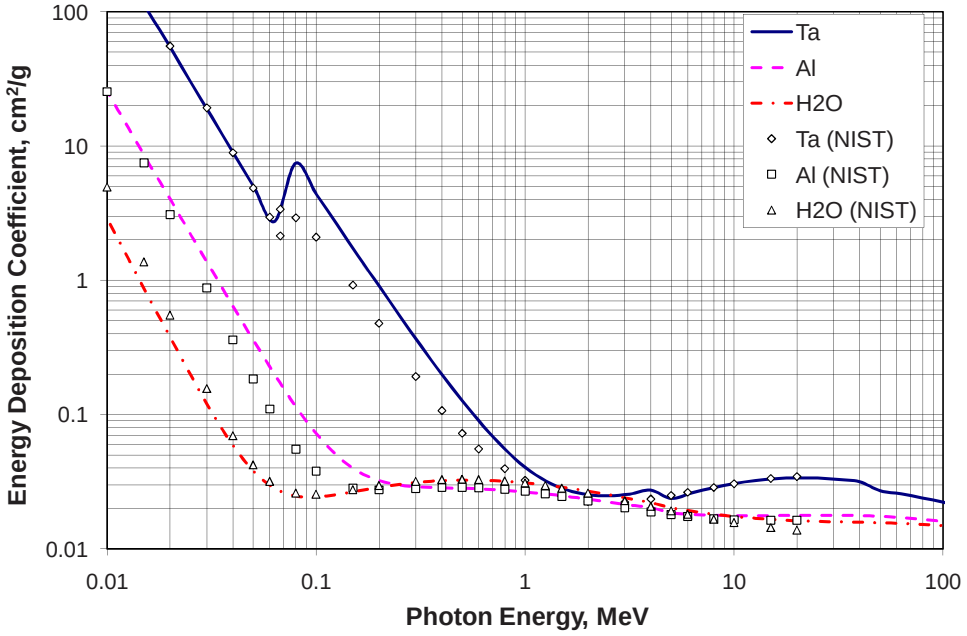

Figure 8: Photon energy deposition coefficients from model compared with NIST values [6].

scattering. The residual energy of an electron, at position s, is given by

$$W(s) = \int_0^R S(E_0, x)dx - \int_0^s S(E_0, x)dx = E_0 - \int_0^s S(E_0, x)dx, \quad s \leq R. \tag{41}$$

For a beam of mono-energetic electrons, it is assumed that the maximum distance traversed is the CSDA range and straggling is neglected. However, the average distance of penetration along the beam axis direction is generally less than the CSDA range due to multiple scattering effects. The average deflection for a unit path length can be defined by the inverse mean free path ($\lambda_{\rm tr}^{-1}$) [9] which yields

$$\langle \cos\theta \rangle = \frac{d\langle z \rangle}{ds} = \exp\left[-\int_0^s \frac{ds'}{\lambda_{\rm tr}(s')} \right] \tag{42}$$

and

$$\langle z(s) \rangle = \int_0^s \exp\left[-\int_0^{s'} \frac{ds''}{\lambda_{\rm tr}(s'')} \right] ds'. \tag{43}$$

In general, $\langle x \rangle$ is defined to be the arithmetic average of the variable x. For electrons, $\langle z(R) \rangle$

is interpreted as an "effective range" or the axial distance at which 50% of the electrons have stopped. In other words, the z-value for which the transmission is 0.5.

A further critical assumption is made by specifying a Gaussian distribution about $\langle z(R)\rangle$, where $\langle z(R)\rangle$ is the distance of peak electron population. In addition, the condition that practically all electrons are stopped at $z = R(E)$ is assumed. This Gaussian represents the variation in electron path length due to multiple scattering effects. By invoking the formula for half-width of the Gaussian distribution, a value for deviation, $\aleph$, is found as [15]

$$\aleph = \frac{R - \langle z(R)\rangle}{2\sqrt{2\ln 2}}. \tag{44}$$

The resultant Gaussian function may be interpreted as the probability that an electron penetrates an axial distance z within increment dz,

$$P(z) = \frac{1}{\aleph\sqrt{2\pi}} \exp\left\{-\frac{[z - \langle z(R)\rangle]^2}{2\aleph^2}\right\}. \tag{45}$$

Integration of the Gaussian function results in an error function prescribing the number of particles having stopped over distance z. The complementary error function [16] results in the corresponding transmission function,

$$\eta(z) = 0.5\left\{1 - \mathrm{erf}\left[\frac{z - \langle z(R)\rangle}{\aleph\sqrt{2}}\right]\right\}. \tag{46}$$

A special algorithm for the standard error function has been utilized in the present code. It has been extracted directly from Winitzki [17].

$$\mathrm{erf}(x) \approx \left[1 - \exp\left(-x^2\frac{ax^2 + \frac{4}{\pi}}{ax^2 + 1}\right)\right]^{1/2},$$

where

$$a \equiv \frac{8}{3\pi}\frac{\pi - 3}{4 - \pi}.$$

For the negative argument, the symmetry relation erf(-x) = -erf(x) is invoked. Sample transmission functions have been calculated for mono-energetic electrons incident on aluminum and are shown in Fig. 9. The results indicate the marked increase of $\langle z\rangle$ as a fraction of R with increasing initial energy.

In addition to specifying the transmission probability of electrons as a function of axial penetration distance z, it is necessary to evaluate the variation of primary electron energy as a function of z. A formula has been developed [10] in terms of the moments of the mass scattering power that expresses, in cylindrical coordinates (z, r), the distance covered for an average electron trajectory having axial distance z and deflection radius r. The moments are calculated as

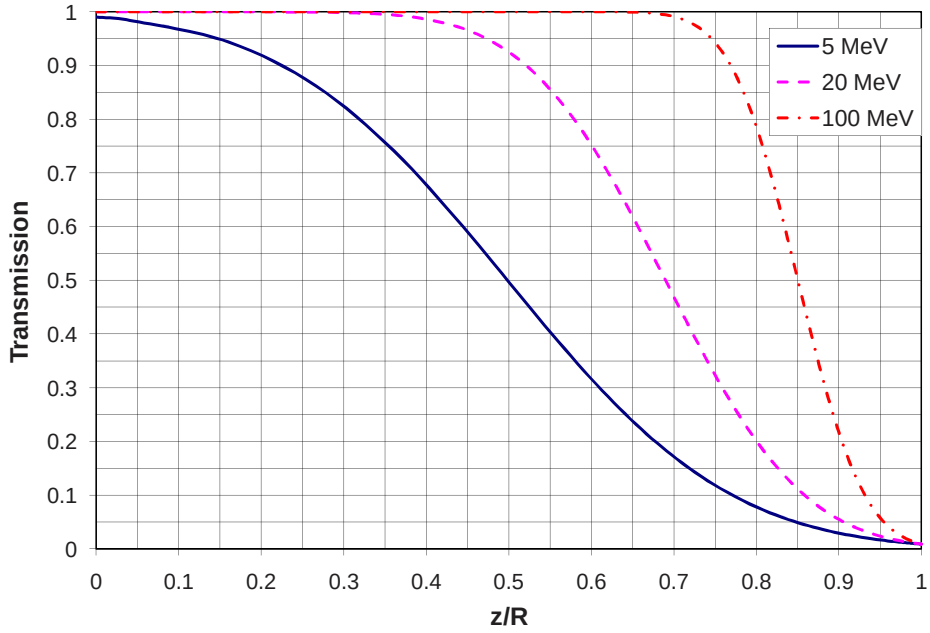

Figure 9: Electron transmission functions in aluminum calculated for three initial energies.

$$a_i = \int_0^z P_s(u)(z-u)^i du, \tag{47}$$

with P_s given by Eq. (22). The moments are then used to derive an equation, details of the derivation are given in Ref. [10], for distance along an average trajectory passing through (z, r),

$$s(z,r) = \int_0^z \left[1 + a_0(z') + \left(\frac{r^2}{a_2(z)} - 1\right)\frac{a_1^2(z')}{a_2(z')}\right]^{1/2} dz'. \tag{48}$$

The quantity $\sqrt{a_2(z)}$ has been identified [10] as the half-width at half-height of the distribution of deflection radius at axial distance z. This observation leads to the inference that a "most typical" trajectory intersects the point $(z, \sqrt{a_2})$. The third term in Eq. (48) then vanishes and an "average mean path" becomes,

$$\langle s(z) \rangle = \int_0^z \sqrt{1 + a_0(z')} dz'. \tag{49}$$

Several of these "typical mean trajectories" have been calculated for a range of incident kinetic energies for the three materials chosen for illustration. The plots of Figs. 10, 11, 12

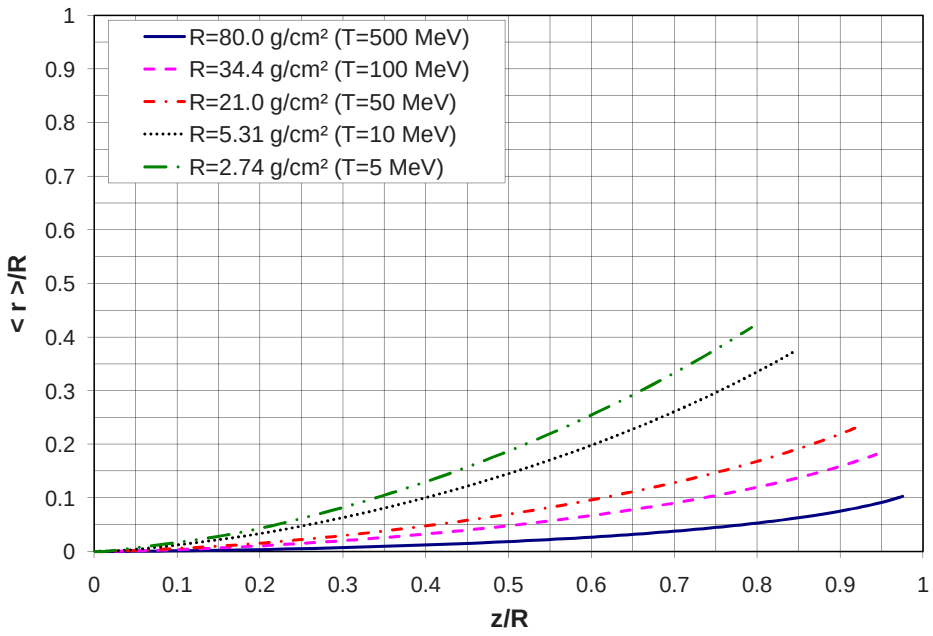

Figure 10: Typical mean trajectories for electrons in H_2O.

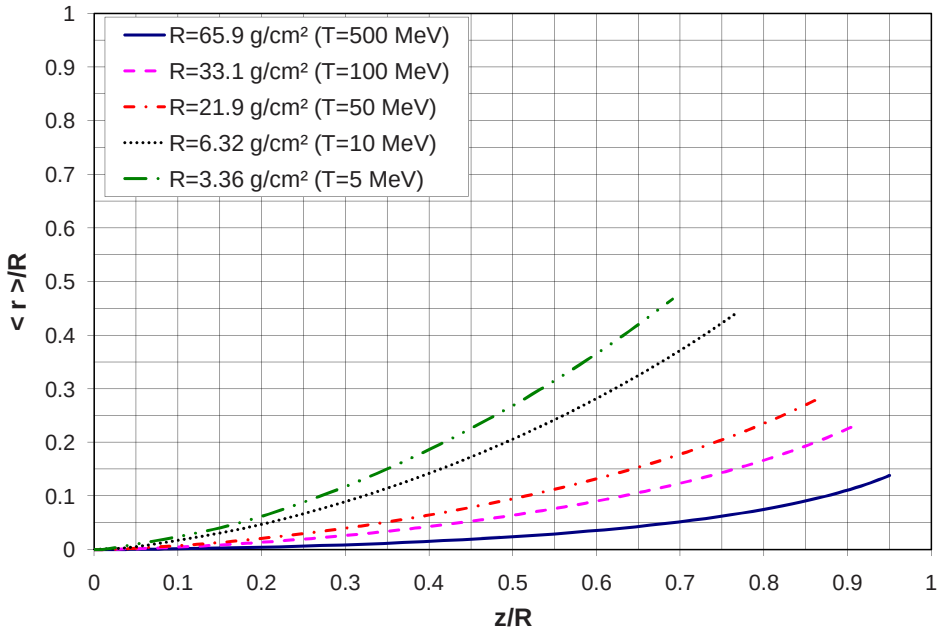

Figure 11: Typical mean trajectories for electrons in aluminum.

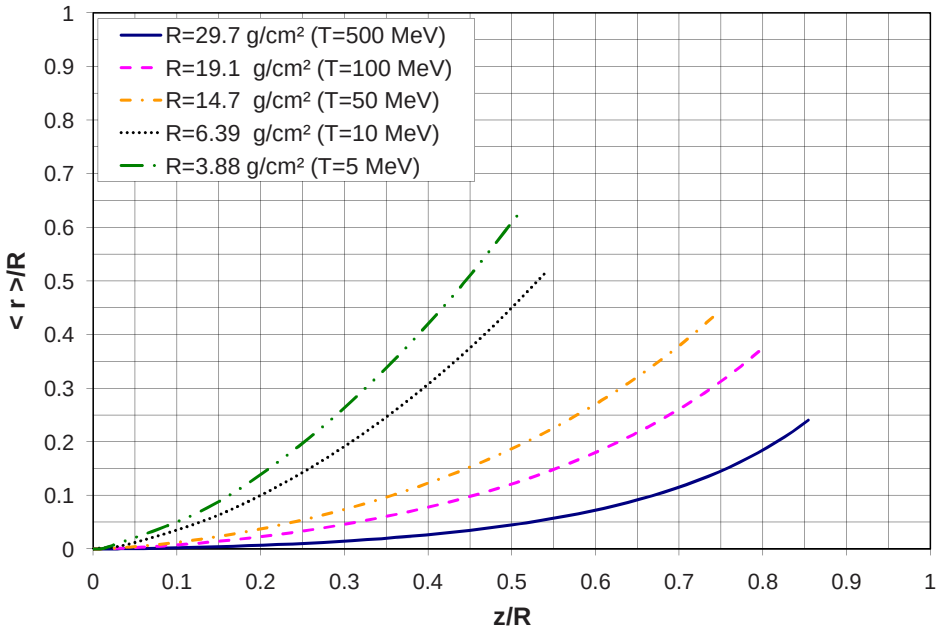

Figure 12: Typical mean trajectories for electrons in tantalum.

display the quantity $\sqrt{a_2}$ versus axial distance z. The curvilinear distance $\langle s(z)\rangle$ along each path is then represented by Eq. (49).

Reference to Eqs. (43) and (49) shows that the relationship between the mean axial distance and average mean path is such that $\langle z\rangle \leq z \leq \langle s\rangle$. The average residual energy $\langle W\rangle$ may be associated with an average distance along a path length $\langle s\rangle$ by again interpolating on a table of CSDA range-energy relations. However, the interpolated value $\langle W\rangle$ reaches zero before $z = R$ is attained since $\langle s\rangle$ is a value that includes average deflection and $z = R$ is the axial distance traveled in the continuous slowing down approximation assuming no angular deflection. The axial penetration, however, may extend beyond the distance at which $\langle W\rangle$ vanishes due to energy straggling. A provision for energy straggling is supplied by activating a power law function of the form

$$\langle W\rangle = A_w(R - z)^k. \tag{50}$$

This formula is invoked somewhat arbitrarily for z-values for which $\langle W\rangle \leq 0.5\ W_{\mathrm{CSDA}}$. When this condition pertains, the constants A_w and k are evaluated by point-slope matching at the z-value where $\langle W\rangle = 0.5\ W_{\mathrm{CSDA}}$. Fig. 13 shows sample normalized residual energy curves calculated for electrons in aluminum at the initial energies of 5 and 50 MeV. The 5 MeV results show considerable divergence of $\langle W\rangle$ from the CSDA loss curve, whereas $\langle W\rangle$ for 50 MeV adheres much more closely to the corresponding CSDA function. The transition to the energy straggling extension is apparent for both cases.

The above transport parameters may be used to devise an expression for the differential flux

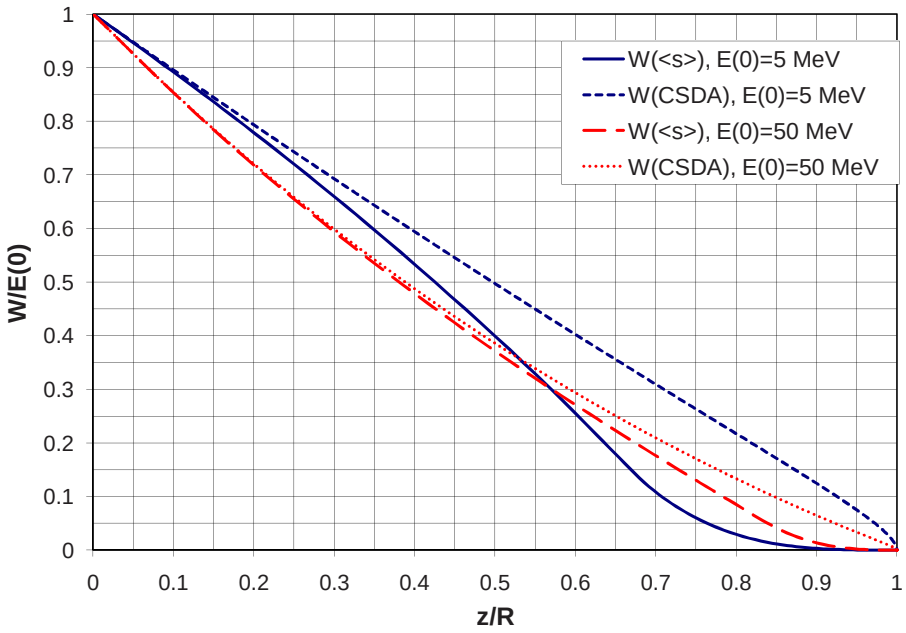

Figure 13: Residual energy functions for electrons in aluminum for 5 and 50 MeV.

spectrum, $\varphi(z,T)$, of electrons at distance z, given the initial spectrum at $z=0$, $\varphi(0,T_0)$. In going from the boundary to distance z, particle number conservation requires that $\varphi(0,T_0)\delta T_0 = \varphi(z,T)\delta T$, where the energy scaling corresponds to that prescribed by the CSDA range-energy relation for the material. In general, δY is defined as a small, finite difference in the value of Y. In addition, the transmission function may be used to account for particles not arriving at z due to interaction not accounted for in the stopping power.

$$\varphi(z,T) = \frac{\varphi(0,T_0)\eta(z,T_0)S(T_0)}{S(T)}. \tag{51}$$

Division of the kinetic energy increments by distance increments leads to the ratio of stopping powers in Eq. (51). Thus, for a slab of thickness w, the differential spectrum of primary electrons may be found at any axial distance $z \leq w$. If primary electrons were the only concern, the calculation could end with Eq. (51). However, bremsstrahlung photons are generated during the transport process. In order to take this process into account, a spatial grid is established within the slab layer. In the present code, a slab layer is assigned a spatial grid, normally of 20 to 30 points, with spacing increasing monotonically according to the following formula,

$$d_i = \left(\frac{i-1}{N-1}\right)^2 w.$$

Here, d_i is the depth in the material slab of the ith point and N is the total number of points in the spatial grid of the slab. The photon source term may then be calculated at each spatial

grid point as

$$\zeta(E_\nu, d_i) = \int_{E_\nu}^{T(d_i)} \varphi_e(T') \frac{d\sigma_{\nu,e}}{dE_\nu} dT' \quad \text{for} \quad 0 < E_\nu \leq T(d_i).$$

Finally, the primary electron spectra provided by the present code are calculated at each spatial grid point as

$$\varphi_{e,i}(d_i, T) = \frac{\varphi(0, E_0)\eta(d_i, E_0)S(E_0)}{S(T)}.$$

Note that the transmission function η has been defined for each initial energy grid value, with the kinetic energy $T(d_i)$ being the corresponding residual energy at d_i. Currently, the code accounts for secondary electron production in the dose calculations by assuming the electron is deposited locally at the point of production.

Implementation of Eq. (51) for the illustrative LEO spectrum [18] normally incident on aluminum provides the results shown in Fig. 14 (the environment spectrum is labeled Z = 0.0). The stopping of low energy electrons and the transfer of high energy electrons to lower energies is evident in the spectral functions at increasing penetration depths. Similar results for the Europa spectrum in aluminum are shown in Fig. 15 using an environment from the Galileo Interim Radiation Electron (GIRE) Model [19]. The much greater penetration and more gradual attenuation is clearly evident for this very high energy environment.

3.2 Photons

In the previous section on cross section evaluation, it was shown that a spectral source term for bremsstrahlung photons may be calculated, Eq. (15). When the differential electron flux spectra have been specified as a function of axial distance z, a corresponding photon flux may be determined using a solution of the radiative transfer equation for an emitting-absorbing medium [14]. In addition to the source function, the total attenuation coefficient is required. The total attenuation coefficient is the sum of the relavant cross sections,

$$\sigma_{\text{Tot}} = \sigma_{\text{PE}} + \sigma_{\text{in}} + \sigma_{\text{pp}}. \tag{52}$$

The photon flux spectrum at each spatial grid point d_i then involves integration of the source term multiplied by the attenuation factor.

$$\varphi_{\nu,i}(d_i, E_\nu) = \int_0^{d_i} \zeta(x, E_\nu) \exp\left[-\sigma_{\text{Tot}}(d_i - x)\right] dx. \tag{53}$$

Photon spectra for the Europa spectrum are illustrated in Fig. 16 and correspond to the electron spectra of the preceding figure. The persistence of higher energy photons at large aluminum depths is indicative of their highly penetrating nature.

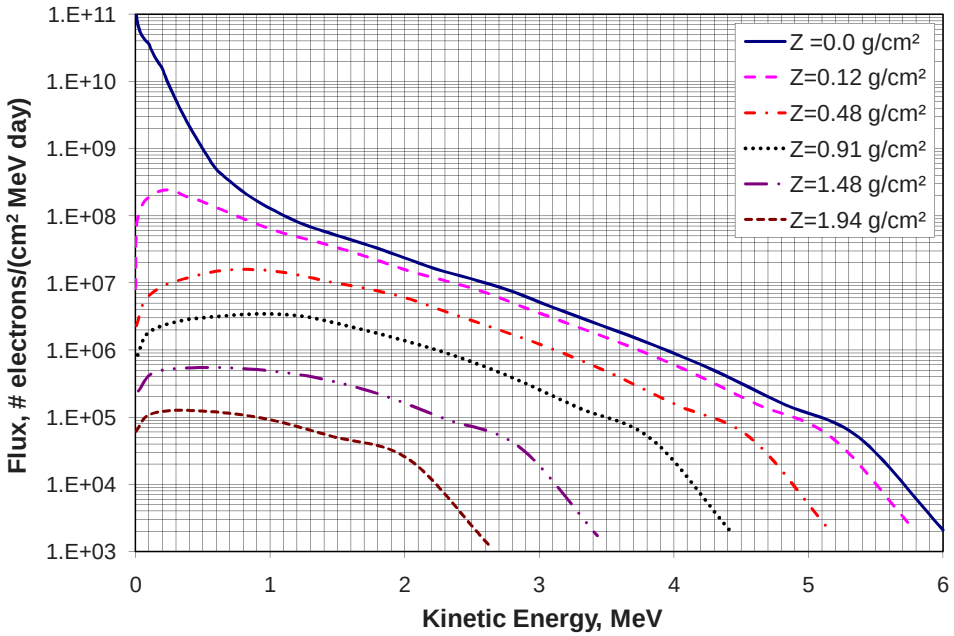

Figure 14: LEO electron spectra at several aluminum thickness values.

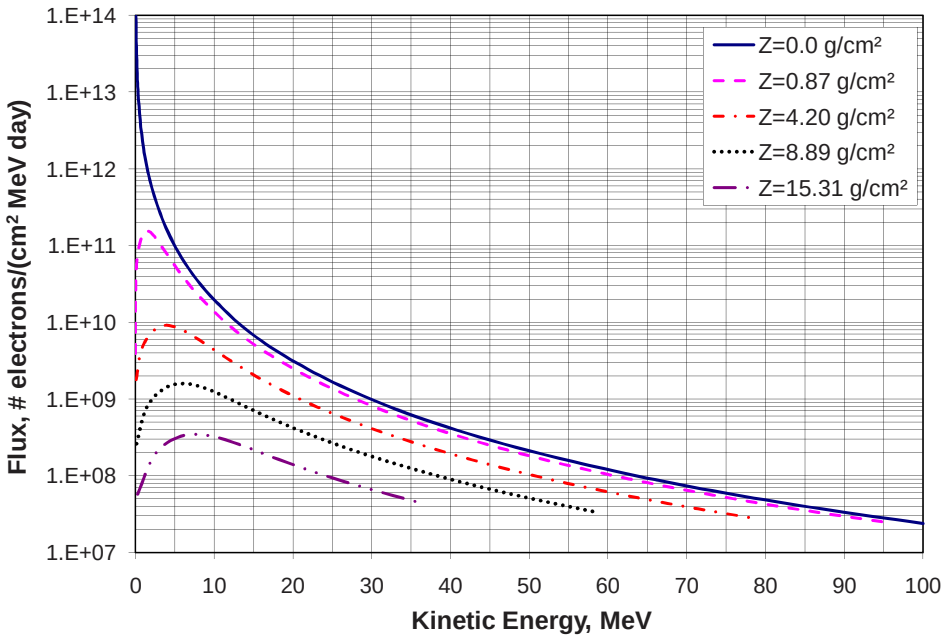

Figure 15: Europa electron spectra at several aluminum thickness values.

3.3 Positrons

Ordinarily, exposure effects due to space environment electrons may be adequately evaluated from specified electron and photon flux values at a given target location. The pair production contribution to the energy absorption coefficient should provide a fair estimate of exposure due to positrons. However, if details of specific positron interactions are of interest, it becomes necessary to include explicit transport of the positrons and their associated annihilation photons. In the present code, source terms and flux for positrons are evaluated, along with source terms for the annihilation photons, in an uncoupled manner with a view toward allowing the user to assess the relative importance of the presence of positrons. The positron source term, $\zeta(E_+, x)$, has already been given as Eq. (37). These antimatter particles have a "sink" term by annihilation with the constituent bound electrons of the medium. This term may be represented as [8]

$$N_e\ \sigma_{\rm ann}(\tau) = \frac{N_e\ \pi r_e^2}{\tau+2}\left[\frac{\tau^2+6\tau+6}{\tau(\tau+2)}h_1 - h_2\right], \tag{54}$$

where N_e is the number of electrons per unit mass of material and $\sigma_{\rm ann}(\tau)$ is the total annihilation cross section, with

$$h_1 = \ln\left[\tau+1+\sqrt{\tau(\tau+2)}\right],$$
$$h_2 = \frac{\tau+4}{\sqrt{\tau(\tau+2)}},$$

and τ representing the positron kinetic energy in rest mass units (0.511 MeV).

Positrons initially at spatial location x_i arriving at $x_i+\delta x$ with energy E_j began traverse of this increment at a higher energy, $E_0 = E(R+\delta x)$, where R is the residual range at $x_i+\delta x$. The CSDA process over the interval δx with no loss of positrons requires that

$$\varphi(E_0, x_i)S(E_0) = \varphi(E_j, x_{i+1})S(E_j). \tag{55}$$

When annihilation takes place, the fraction of positrons from the incident spectrum lost in distance δx is

$$A_T(\delta x) = \exp\left\{-\int_0^{\delta x} N_e\ \sigma_{\rm ann}\left[E\left(R_j+x'\right)\right]dx'\right\}. \tag{56}$$

The positrons transmitted through interval δx is then

$$\varphi^{(t)}(E_j, x_i+\delta x) = \rho_S A_T(\delta x)\varphi\left[E\left(R_j+\delta x\right), x_i\right], \tag{57}$$

with

$$\rho_S = \frac{S\left[E\left(R_j+\delta x\right)\right]}{S(E_j)}.$$

Additional contributions to the positron flux at $x_{i+1} \equiv x_i + \delta x$ arise from the distributed sources in the interval that must include an additional annihilation factor, A_S.

$$\varphi^{(s)}\left(E_j, x+\delta x\right) = \int_0^{\delta x} \zeta[E(R+x^{'}), x_i + x^{'}] A_S(x^{'}) dx^{'}, \tag{58}$$

with

$$A_S(x^{'}) = \exp\left\{ -\int_0^{x^{'}} N_e\ \sigma_{\rm ann}\left[E\left(R_j + x^{''}\right)\right] dx^{''} \right\}. \tag{59}$$

Here, A_S is the fraction of positrons lost from the positrons created in the distance increment.

The total positron flux, $\varphi_{e^+} = \varphi^{(t)} + \varphi^{(s)}$, is calculated in the code by simple numerical integration procedures applied to each of the established spatial grid intervals. Results for the Europa spectrum for selected thicknesses in aluminum are shown in Fig. 17 and may be compared with the corresponding photon flux of Fig. 16. It is seen that the positron flux is a relatively small fraction of the governing photon field and that the uncoupled calculation is justified.

When the positrons are annihilated, photons are generated in accordance with the differential cross section [8].

$$\frac{d\sigma_{\rm ann}}{dE_\nu} = \frac{\pi r_e^2}{\tau(\tau+2)}\left[q(\kappa) + q(\tau+2-\kappa)\right], \tag{60}$$

where

$$q(x) \equiv \frac{1}{x}\left(\tau + 2 + 2\frac{\tau+1}{\tau+2} - \frac{1}{x}\right) - 1,$$

with τ and κ being the positron kinetic energy and the photon energy, respectively, in units of electron rest mass. The annihilation photons are restricted by kinematics to an energy range of

$$\frac{m_e}{1+a'} \le E_{\nu,{\rm ann}} \le \frac{m_e}{1-a'}, \tag{61}$$

where

$$a' \equiv \sqrt{\frac{\tau}{\tau+2}}.$$

Finally, a source term for the annihilation photons per unit mass of material may be expressed as

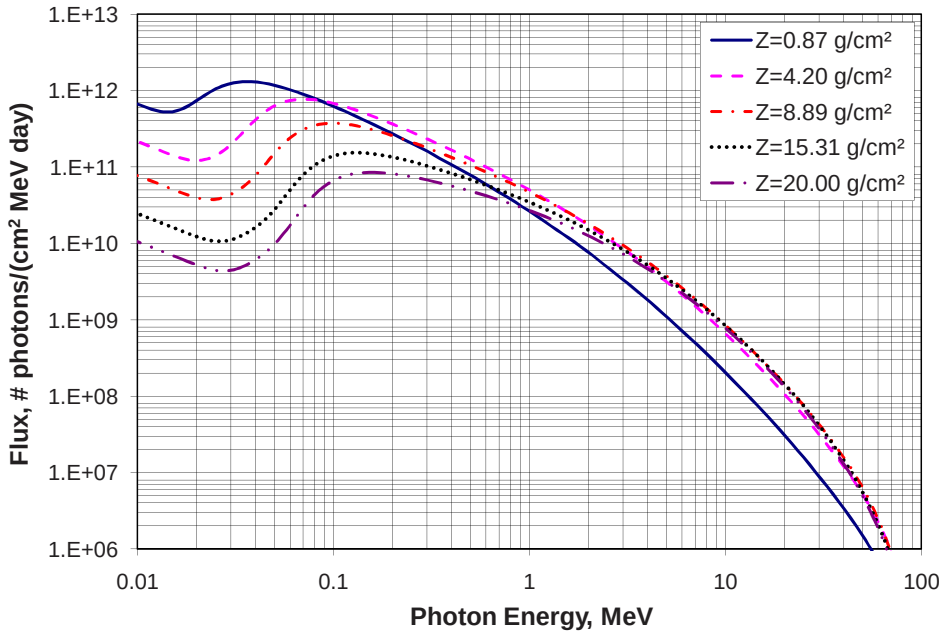

Figure 16: Photon spectra from Europa electrons [19] at several aluminum thickness values.

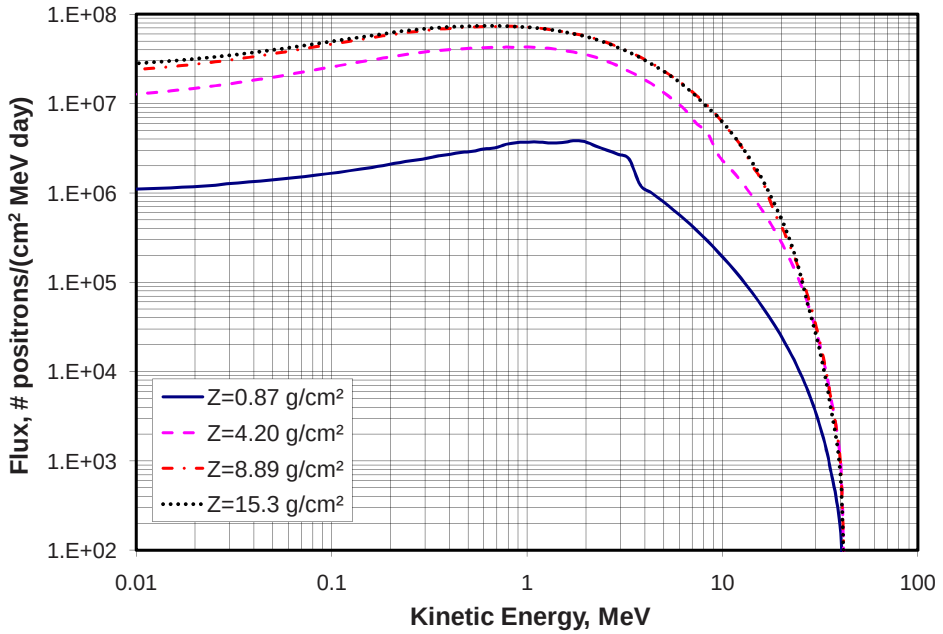

Figure 17: Positron flux at selected thicknesses in aluminum for Europa spectrum [19].

$$\zeta_{\nu,\mathrm{ann}}(E_\nu, x) = \int_{T_{\min}}^{T_{\max}} \varphi(E_+, x) \frac{d\sigma_{\mathrm{ann}}}{dE_\nu} dT_+. \tag{62}$$

Production of annihilation photons occurs with highest probability near the electron/positron rest mass energy. For the Europa case of Fig. 17, the annihilation photon source terms calculated according to Eq. (62) are shown in Fig. 18 and exhibit the expected peak at 0.511 MeV. Since this contribution is small relative to the other processes, these photons are not transported in the present formulation.

4 Dosimetric Calculations and Comparisons

The conventional radiation dose for ionizing radiations in matter is defined as the energy imparted to a mass element of the material by the particles traversing the elemental mass. In general, only energetic charged particles are responsible for the energy transfer. The "dose" attributed to uncharged particles (e.g. photons, neutrons) results from the charged particles generated within the medium by the neutrals.

4.1 Electron and Photon Dose Evaluation

Energy deposition of electrons is calculated by multiplying the local flux (differential in energy) by the total stopping power and integrating over energy. The dose at a given location is given by

$$D_e(x) = \int_0^\infty \varphi_e(x, E) S(E) dE. \tag{63}$$

In Eq. (63), E represents the electron energy at position x. The local differential flux, φ_e, has units of electrons/(cm^2 MeV). The stopping power, S, has units of MeV cm^2/g, while the units of D_e are MeV/g which may be converted to cGy or rads upon multiplication by the conversion factor 1.602×10^{-8}. For the photons, absorbed dose is characterized by the energy deposition coefficient, μ_{en}, which is described in Eq. (39) and is expressed herein as a mass absorption coefficient with units cm^2/g. The dose attributed to photons is then

$$D_\nu(x) = \int_0^\infty \mu_{\mathrm{en}}\ E_\nu\ \varphi_\nu(E_\nu, x) dE_\nu. \tag{64}$$

The use of μ_{en} to calculate effective photon dose (as in the present version of the code) is a simplistic approximation method that has been widely used and considered to be an adequate representation of this dose contribution [3, 6]. This approximation assumes that all the energy deposited by photons is deposited by charged particles at the point of their production. A more direct evaluation would be to use the appropriate cross sections for generation of secondary

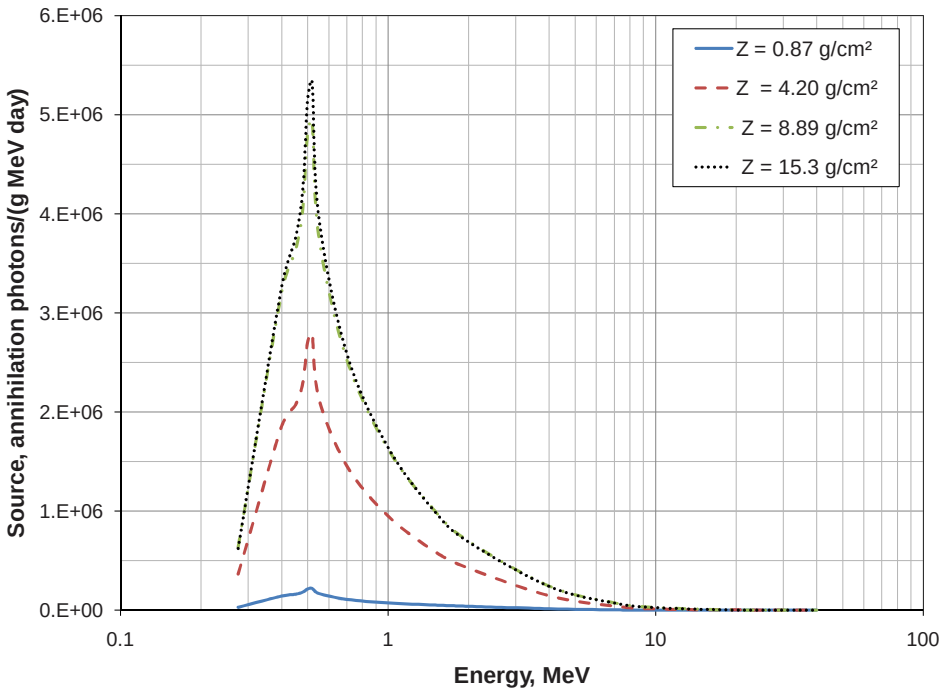

Figure 18: Annihilation photon source for Europa spectrum [19] in aluminum.

electrons (σ_{PE}, σ_{in}, and σ_{pp}) to compute respective source terms in the manner expressed in Eq. (37). The corresponding flux terms could then be determined using procedures analogous to that described for the positron transport in Eqs. (54)-(58). Such modifications may be considered for future upgrades if the additional complexity appears to be warranted.

4.2 Sample Calculations and Comparisons

Calculations performed with the present code were selected to examine the behavior of trapped electron spectra interacting with light and heavy materials. The chosen electron environment spectra (boundary conditions) are shown in Figs. 14 and 15 and represent, respectively, the environment in LEO (400 km, 51° inclination) [18] and the environment in the vicinity of the orbit of the Jovian moon Europa [19]. The initial environment is shown as the curves labeled Z=0.0 in Figs. 14 and 15, along with the flux spectra at various depths in aluminum. After transport through the shield medium, the doses have been evaluated in silicon to simulate exposure of a solid state device.

The Integrated TIGER Series (ITS) Monte Carlo code [20] was used to calculate dose for the LEO spectrum electrons on aluminum at normal incidence for several depths. The identical scenario was used with the LaRC deterministic code and the results are compared in Fig. 19. The LaRC code gives generally lower values for the dose versus depth functions than the Monte Carlo results, but the functional behavior is very similar. Greater differences are to be expected for

the low energy spectra of LEO because scattering processes are more prominent in the transport process and are treated differently in the two calculations.

A second exercise using the LEO spectrum was performed using the SPENVIS space environment website that incorporates the application code SHIELDOSE-2 that is based on results from ITS, parameterized for several simple geometries [18]. The geometry selected is that of the semi-infinite slab adjacent to an isotropic field of energetic electrons having the same LEO energy spectrum previously used. For the LaRC comparison calculation, a dose versus depth function was generated for normal incidence on aluminum. A solid angle integration was then performed over a directional hemisphere about a target point on the shielded side of the slab. For a slab of thickness w, the calculation may be expressed as

$$D(w) = \frac{1}{4\pi} \int_0^{2\pi} \int_0^{\pi} D\left(\frac{w}{\cos\theta}\right) \sin\theta d\theta d\phi = \frac{1}{2} \int_0^1 D\left(\frac{w}{\cos\theta}\right) d\cos\theta. \tag{65}$$

The comparison of the LaRC results with those of SPENVIS are shown in Fig. 20 and again indicate that the LaRC results for total dose are generally lower than those based on the Monte Carlo calculation. This adds credibility to the previous normal incidence calculations of Fig. 19.

For higher energy electron spectra, sample application comparisons have been made for a Jovian electron environment generated by the NASA-JPL GIRE model [19]. The relevant spectrum is shown in Fig. 15 as the curve labeled Z = 0.0 and represents electron flux in Jupiter's equatorial plane at the average orbital distance of Europa. The normal incidence on a semi-infinite slab scenario was used for the materials aluminum, tantalum, and copper-tungsten (50%-50%) alloy. The previous LEO spectrum exhibited very few electrons above 5 MeV, whereas the Europa electrons may have substantial population up to and beyond 100 MeV.

The dose versus depth curves for the Europa spectrum are given in Figs. 21, 22, and 23 for the specified materials. In general, the LaRC deterministic calculations show improved agreement with the corresponding Monte Carlo results compared to the lower energy LEO environment. The range of scaled thickness for the Europa cases is from 0.5 to 20 g/cm^2. It is seen that electron stopping is practically complete at the end of this thickness range, after which the bremsstrahlung contribution dominates.

5 Concluding Remarks

The electron/photon transport code described here has been developed with a view toward simplicity and speed in analysis of exposure from space environment electrons. In its present form, the code may be implemented to great advantage in shield material trade studies, numerical and statistical experiments, uncertainty analyses, etc., despite some observed differences with Monte Carlo comparisons. Numerous comparative calculations, in addition to those reported here, have been performed with similar degrees of agreement as those presented in the text. In particular, calculations for the trapped Jovian environment compare more favorably with corresponding Monte Carlo results than do the comparisons for the much lower energy-range

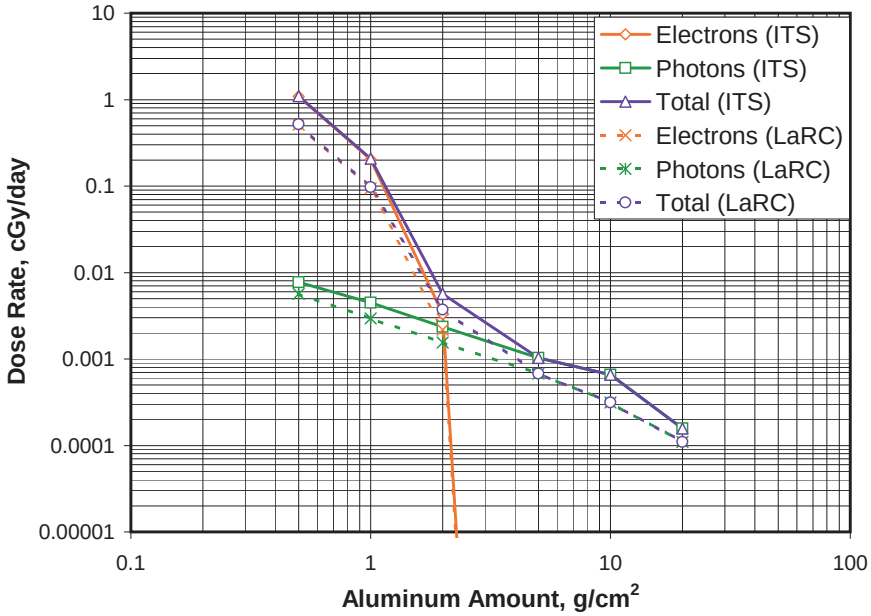

Figure 19: Comparison of dose rate results in aluminum for the LaRC model with the ITS [20] model from a LEO spectrum [18].

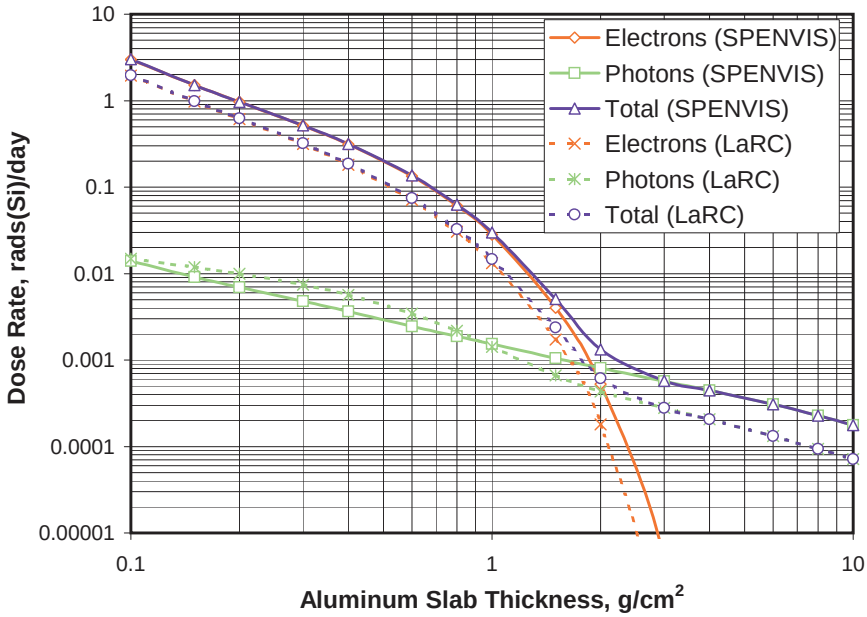

Figure 20: Comparison of dose rate results in aluminum for the LaRC model with the SPENVIS [18] model from a LEO spectrum [18].

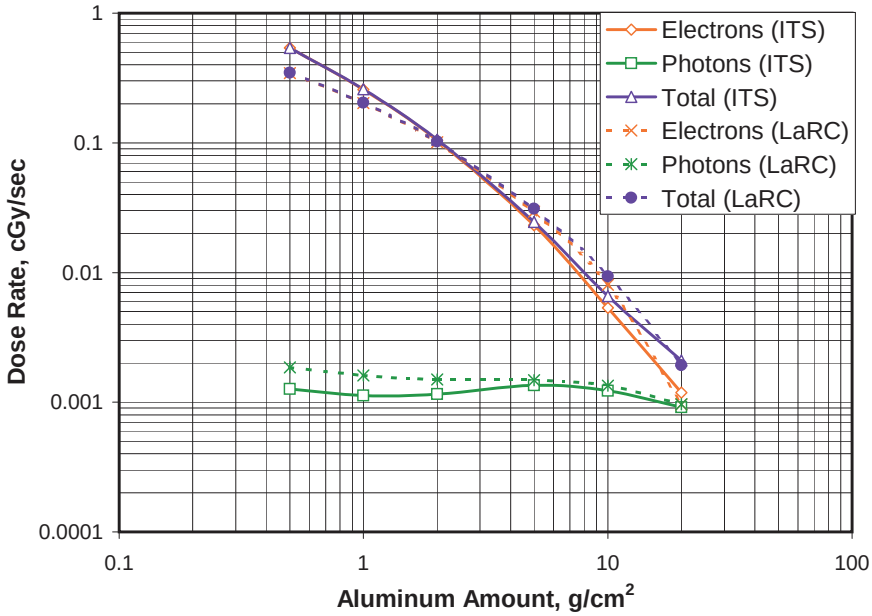

Figure 21: Comparison of dose rate results in aluminum for the LaRC model with the ITS [20] for Europa spectrum [19].

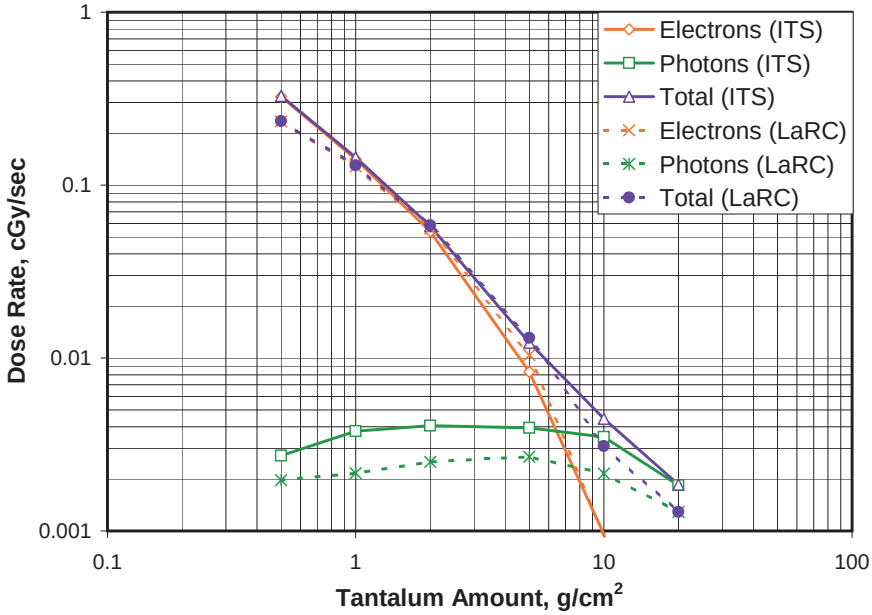

Figure 22: Comparison of dose rate results in tantalum for the LaRC model with the ITS [20] for Europa spectrum [19].

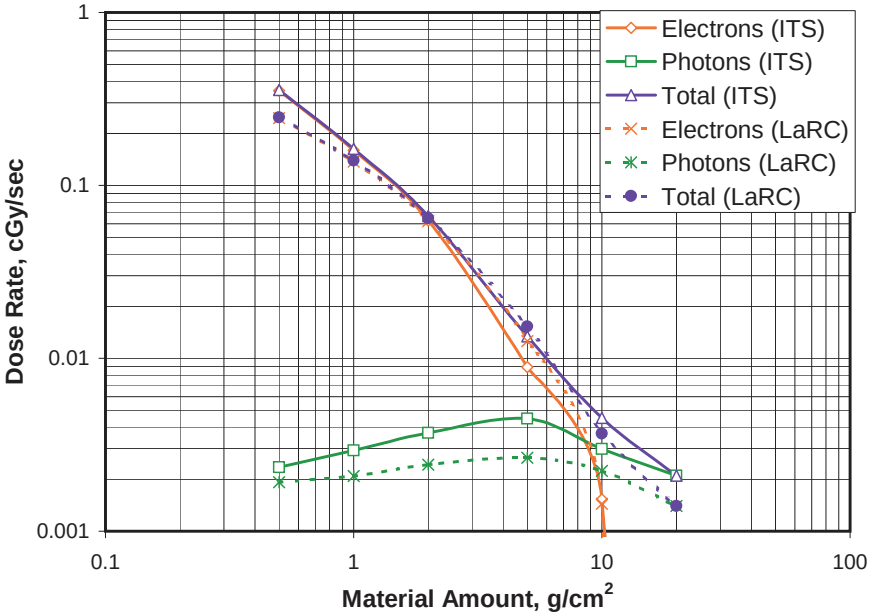

Figure 23: Comparison of dose rate results in W-Cu alloy for the LaRC model with the ITS [20] for Europa spectrum [19].

spectra of LEO. This fact suggests that the deterministic formulas for low-energy scattering should be improved in future versions.

The present code may be used in a variety of space mission applications, but may also be considered as developmental for several reasons. The various cross section comparisons with NIST calculations show several instances where the LaRC code cross sections may be improved by introducing selective correction terms, even though the cross section deviations noted have little impact on final exposure results. With regard to transport, the present code is amenable to immediate extension to a two-dimensional axi-symmetric representation. In addition, more explicit details pertaining to very high energy processes involving positrons and their annihilation photons may be obtained by a formal coupling of these species to the general electron/photon transport. Although no significant errors are indicated as a result of the decoupling of positron and annihilation photon transport for the Jovian spectral environments, use of the present code for high energy beam simulation or cosmic ray shower analysis would most likely require full coupling of these processes. It is therefore natural to anticipate code upgrades and extensions in the near future.

References

[1] J. W. Wilson, F. F. Badavi, F. A. Cucinotta, J. L. Shinn, G. D. Badhwar, R. Silberberg, C. H. Tsao, L. W. Townsend and R. K. Tripathi, HZETRN: Description of a free-space ion and nucleon transport and shielding computer program, NASA TP-3495, (1995).

[2] J. E. Nealy, B. M. Anderson, F. A. Cucinotta, J. W. Wilson, R. Katz and C. K. Chang, Transport of Space Environment Electrons: A Simplified Rapid-Analysis Computational Procedure, NASA TP-2002-211448, (2002).

[3] D. W. Anderson, *Absorption of Ionizing Radiation* (University Park Press, Baltimore, 1984).

[4] R. M. Sternheimer and R. F. Peierls, General expression for the density effect for the ionization loss of charged particles, Physical Review B **3**, 3681 (1971).

[5] P. Sigmund, Low-speed limit of Bohr's stopping-power formula, Physical Review A **54**, 3113 (1996).

[6] National Institute of Standards and Technology (NIST), `http://www.nist.gov`.

[7] H. W. Koch and J. W. Motz, Bremsstrahlung cross-section formulas and related data, Reviews of Modern Physics **31**, 920 (1959).

[8] I. Kawrakow and D. W. O. Rogers, The EGSnrc Code System: Monte Carlo Simulation of Electron and Photon Transport, NRCC Report PIRS-701, (2009).

[9] D. Liljequist and M. Ismail, Transport mean free path related to trajectory patterns: Comparison of nonrelativistic and highly relativistic electron penetration through matter, Journal of Applied Physics **62**, 342 (1987).

[10] I. A. D. Bruinvis, W. A. F. Mathol and P. Andreo, Inclusion of electron range straggling in the Fermi-Eyges multiple-scattering theory, Physics in Medicine and Biology **34**, 491 (1989).

[11] X. A. Li and D. W. O. Rogers, Electron mass scattering powers: Monte Carlo and analytical calculations, `http://www.irs.inms.nrc.ca/papers/MSP95/msp.html`.

[12] J. W. Motz, H. A. Olsen and H. W. Koch, Pair production by photons, Reviews of Modern Physics **41**, 581 (1969).

[13] C. Leroy and P.-G. Rancoita, *Principles of Radiation Interaction in Matter and Detection* (World Scientific, New Jersey, 2004).

[14] S. Chandrasekhar, *Radiative Transfer* (Dover Publications, New York, 1960).

[15] S. Brandt and G. Cowan, *Data Analysis* (Springer-Verlag, New York, 1999).

[16] G. B. Arfken and H. J. Weber, *Mathematical Methods for Physicists* (Academic Press, San Diego, 2001).

[17] S. Winitzki, A handy approximation for the error function and its inverse, `http://homepages.physik.uni-muenchen.de/~Winitzki/erf-approx.pdf`.

[18] SPENVIS: The European Space Agency (ESA) SPace ENVIronment System, `http://www.spenvis.oma.be/`.

[19] H. B. Garrett, I. Jun, J. M. Ratliff, R. W. Evans, G. A. Clough and R. W. McEntire, Galileo Interim Radiation Electron (GIRE) Model, JPL Pub. 03-006, (2003).

[20] J. Halbleib, R. Kensek, G. Valdez, T. Mehlhorn, S. Seltzer and M. Berger, ITS Version 3.0: The Integrated TIGER Series of Coupled Electron/Photon Monte Carlo Transport Codes, Sandia National Laboratory SAND91-1634, (1992).

Appendix A Input File of Atomic Data

Table 2: Input File of Atomic Data used in the Electron Transport code. Values appearing in italics for the material density, ρ, indicate the value corresponds to the condensed phase of the material.

Sym	Z	A	ρ (g/cm^3)	I (eV)		Sym	Z	A	ρ (g/cm^3)	I (eV)
H	1	1.008	*0.071*	19.2		Ag	47	107.868	10.5	470
He	2	4.003	*0.122*	41.8		Cd	48	112.41	8.65	469
Li	3	6.941	0.534	40		In	49	114.82	7.31	488
Be	4	9.012	1.848	63.7		Sn	50	118.71	5.75	488
B	5	10.81	2.37	76		Sb	51	121.75	6.691	487
C	6	12.011	2	78		Te	52	127.6	6.24	485
N	7	14.007	*0.808*	82		I	53	126.905	4.93	491
O	8	15.999	*1.14*	95		Xe	54	131.29	*3.52*	482
F	9	18.998	*1.108*	115		Cs	55	132.905	1.873	488
Ne	10	20.179	*1.207*	137		Ba	56	137.33	3.5	491
Na	11	22.99	0.971	149		La	57	138.906	6.145	501
Mg	12	24.305	1.738	156		Ce	58	140.12	6.657	523
Al	13	26.982	2.699	166		Pr	59	140.98	6.7	535
Si	14	28.086	2.33	173		Nd	60	144.24	6.9	546
P	15	30.974	2	173		Pm	61	145	7.22	560
S	16	32.06	2	180		Sm	62	150.36	7.5	574
Cl	17	35.453	*1.56*	174		Eu	63	151.96	5.243	580
Ar	18	39.948	1	188		Gd	64	157.25	7.9	591
K	19	39.098	0.862	190		Tb	65	158.925	8.229	614
Ca	20	40.08	1.55	191		Dy	66	162.5	8.55	628
Sc	21	44.956	2.989	216		Ho	67	164.93	8.795	650
Ti	22	47.88	4.54	233		Er	68	167.26	9.066	658
V	23	50.942	6.11	245		Tm	69	168.934	9.321	674
Cr	24	51.996	7.19	257		Yb	70	173.04	6.9	684
Mn	25	54.938	7.3	272		Lu	71	174.967	9.84	694
Fe	26	55.847	7.874	286		Hf	72	178.49	13.31	705
Co	27	58.932	8.9	297		Ta	73	180.948	16.654	718
Ni	28	58.69	8.902	311		W	74	183.85	19.3	727
Cu	29	63.546	8.96	322		Re	75	186.207	21.02	736
Zn	30	65.39	7.133	330		Os	76	190.2	22.57	746
Ga	31	69.72	5.904	334		Ir	77	192.22	22.42	757
Ge	32	72.59	5.323	350		Pt	78	195.08	21.45	790
As	33	74.922	1.97	347		Au	79	196.967	19.3	790
Se	34	78.96	4.79	348		Hg	80	200.59	*13.546*	800
Br	35	79.904	*3.12*	357		Tl	81	204.383	11.85	810
Kr	36	83.8	1	352		Pb	82	207.2	11.35	823
Rb	37	85.468	1.532	363		Bi	83	208.98	9.747	823
Sr	38	87.62	2.54	366		Po	84	209	9.32	830
Y	39	88.906	4.469	379		At	85	210	1	825
Zr	40	91.224	6.506	393		Rn	86	222	*4.4*	794
Nb	41	92.906	8.57	417		Fr	87	223	1	827
Mo	42	95.94	10.22	424		Ra	88	226.025	5	826
Tc	43	98	11.5	428		Ac	89	227.028	10.07	841
Ru	44	101.07	12.41	441		Th	90	232.038	11.72	847
Rh	45	102.906	12.41	449		Pa	91	231.036	15.37	878
Pd	46	106.42	12.02	470		U	92	238.029	18.95	890

REPORT DOCUMENTATION PAGE

Form Approved
OMB No. 0704-0188

1. REPORT DATE *(DD-MM-YYYY)*	2. REPORT TYPE	3. DATES COVERED *(From - To)*
01-01-2010	Technical Publication	

4. TITLE AND SUBTITLE
A Deterministic Transport Code for Space Environment Electrons

5a. CONTRACT NUMBER

5b. GRANT NUMBER

5c. PROGRAM ELEMENT NUMBER

6. AUTHOR(S)
Nealy, John E.; Chang, Chie K,.; Norman, Ryan B.; Blattnig, Steve R.; Badavi, Francis F.; Adamczyk, Anne M.

5d. PROJECT NUMBER

5e. TASK NUMBER

5f. WORK UNIT NUMBER
651549.02.07.01

7. PERFORMING ORGANIZATION NAME(S) AND ADDRESS(ES)
NASA Langley Research Center
Hampton, VA 23681-2199

8. PERFORMING ORGANIZATION REPORT NUMBER
L-19795

9. SPONSORING/MONITORING AGENCY NAME(S) AND ADDRESS(ES)
National Aeronautics and Space Administration
Washington, DC 20546-0001

10. SPONSOR/MONITOR'S ACRONYM(S)
NASA

11. SPONSOR/MONITOR'S REPORT NUMBER(S)
NASA/TP-20010-216168

12. DISTRIBUTION/AVAILABILITY STATEMENT
Unclassified - Unlimited
Subject Category 93
Availability: NASA CASI (443) 757-5802

13. SUPPLEMENTARY NOTES

14. ABSTRACT

A deterministic computational procedure has been developed to describe transport of space environment electrons in various shield media. This code is an upgrade and extension of an earlier electron code. Whereas the former code was formulated on the basis of parametric functions derived from limited laboratory data, the present code utilizes well established theoretical representations to describe the relevant interactions and transport processes. The shield material specification has been made more general, as have the pertinent cross sections. A combined mean free path and average trajectory approach has been used in the transport formalism. Comparisons with Monte Carlo calculations are presented.

15. SUBJECT TERMS
Space radiation; Radiation transport; Electronics; Electrons; Photons

16. SECURITY CLASSIFICATION OF:			17. LIMITATION OF ABSTRACT	18. NUMBER OF PAGES	19a. NAME OF RESPONSIBLE PERSON
a. REPORT	b. ABSTRACT	c. THIS PAGE			STI Help Desk (email: help@sti.nasa.gov)
					19b. TELEPHONE NUMBER *(Include area code)*
U	U	U	UU	51	(443) 757-5802